

1 **Fate-resolved gene regulatory signatures of individual B lymphocytes in the early  
2 stages of Epstein-Barr Virus infection**

3  
4 Elliott D. SoRelle<sup>1,2\*</sup>, Joanne Dai<sup>1,3</sup>, Nicolás M. Reinoso-Vizcaino<sup>1</sup>, Ashley P. Barry<sup>1</sup>, Cliburn  
5 Chan<sup>2</sup>, & Micah A. Luftig<sup>1\*</sup>

6  
7 <sup>1</sup> Department of Molecular Genetics and Microbiology, Duke Center for Virology, Duke University School  
8 of Medicine, Durham, NC 27710

9 <sup>2</sup> Department of Biostatistics and Bioinformatics, Duke University School of Medicine, Durham, NC 27710

10 <sup>3</sup> Current address: Amgen Inc., 1120 Veterans Blvd, South San Francisco, CA 94080

11  
12 \*Corresponding Authors: Elliott D. SoRelle & Micah A. Luftig

13  
14 **Abstract**

15 Epstein-Barr Virus (EBV) infection of B lymphocytes elicits diverse host responses via complex,  
16 well-adapted transcriptional control dynamics. Consequently, this host-pathogen interaction  
17 provides a powerful system to explore fundamental cellular processes that contribute to  
18 consensus fate decisions including cell cycle arrest, apoptosis, proliferation, and differentiation.  
19 Here we capture these responses and fates with matched single-cell transcriptomics and  
20 chromatin accessibility, from which we construct a genome-wide multistate model of early  
21 infection dynamics. Notably, our model captures a previously uncharacterized EBV<sup>+</sup> analog of a  
22 multipotent activated precursor state that can yield early memory B cells. We also find that a  
23 marked global reduction in host chromatin accessibility occurs during the first stages of infection  
24 in subpopulations of EBV<sup>+</sup> cells that display senescent and pre-apoptotic hallmarks induced by  
25 innate antiviral sensing and proliferation-linked DNA damage. However, cells in proliferative  
26 infection trajectories exhibit greater accessibility at select host sites linked to B cell activation and  
27 survival genes as well as key regions within the viral genome. To further investigate such loci, we  
28 implement a bioinformatic workflow (crisp-ATAC) to identify phenotype-resolved regulatory  
29 signatures. This customizable method applies user-specified logical criteria to produce genome-  
30 wide single-cell ATAC- and ChIP-seq range intersections that are used as inputs for *cis*-linkage  
31 prediction and ontology tools. The resulting tri-modal data yield exquisitely detailed hierarchical  
32 perspectives of the transforming regulatory landscape during critical stages of an oncogenic viral  
33 infection that simulates antigen-induced B cell activation and differentiation. We anticipate these  
34 resources will guide investigations of gene regulatory modules controlling EBV-host dynamics, B  
35 cell effector fates, and lymphomagenesis. To demonstrate the utility of this resource, this work  
36 concludes with the discovery of EBV infection dynamics in FCRL4<sup>+</sup> / TBX21<sup>+</sup> Tissue-Like Memory  
37 B cells, an unconventional subset with notable associations to numerous immune disorders.

40 **Introduction**

41

42 Epstein-Barr Virus (EBV) is an oncogenic gammaherpesvirus present in >90% of adults  
43 ([Rickinson and Kieff, 2007](#)) and associated with up to 2% of human cancers ([Cohen et al., 2011](#)).  
44 Recent reports have also provided epidemiological and mechanistic evidence supporting an  
45 etiological role for EBV in multiple sclerosis (MS) ([Bjornevik et al., 2022](#); [Lanz et al., 2022](#)). In its  
46 initial stages, EBV infection within primary B lymphocytes manifests an array of host and viral  
47 programs. Upon entry into the host cell, the linear dsDNA viral genome rapidly circularizes to form  
48 an episome that is retained within the nucleus ([Lindahl et al., 1976](#); [Nonoyama and Pagano,](#)  
49 [1972](#)). Within hours to days, host innate immune responses are generated to restrict viral  
50 progression ([Lünemann et al., 2015](#); [Martin et al., 2007](#); [Smith et al., 2013](#); [Tsai et al., 2011](#)).  
51 Simultaneously, viral genes are expressed to counteract host defenses ([Ressing et al., 2015](#)), co-  
52 opt B cell-intrinsic activation and proliferation ([Calender et al., 1987](#); [Thorley-Lawson, 2001](#);  
53 [Thorley-Lawson and Mann, 1985](#)), and attenuate DNA damage and stress responses instigated  
54 by virus-induced growth ([McFadden et al., 2016](#); [Nikitin et al., 2010](#)). A consequence of these  
55 intimately adapted host-pathogen dynamics is that EBV infection can precipitate diverse  
56 responses and outcomes for host B cells. These include unsuccessful infection routes resulting  
57 from effective antiviral restriction and DNA damage-induced growth arrest as well as successful  
58 infection leading to immortalization *in vitro* ([Bird, 1981](#); [Henle et al., 1967](#); [Pope et al., 1968](#); [Zhao](#)  
59 [et al., 2011](#)) or lifelong latency *in vivo* within memory B cells ([Babcock, 1998](#); [Longnecker et al.,](#)  
60 [2013](#); [Miyashita et al., 1997](#)) that retain oncogenic potential ([Raab-Traub, 2007](#); [Thorley-Lawson](#)  
61 [and Gross, 2004](#)).

62 Since its discovery in 1964 as the first human tumor virus ([Epstein et al., 1964](#); [Young and](#)  
63 [Rickinson, 2004](#)), extensive research has revealed the molecular means by which EBV  
64 establishes infection and underlies various malignancies. The entire EBV genome is ~172  
65 kilobases and contains at least 80 protein-coding sequences including six EBV nuclear antigens  
66 (EBNAs); several latent membrane proteins (LMPs); and loci that encode replicative and  
67 transcriptional machinery as well as structural proteins. The EBV genome also contains functional  
68 non-coding RNAs: the BHRF and BART microRNAs and the EBV-encoding regions (EBERs)  
69 ([Rickinson and Kieff, 2007](#); [Young et al., 2007](#)).

70 EBNAs are especially important in establishing distinct forms of latency depending on their  
71 combinatorial expression ([Price and Luftig, 2015](#)). EBNA1 is a transcription factor (TF) that is  
72 essential for viral genome maintenance and B cell transformation and ubiquitously binds and  
73 epigenetically regulates host chromatin ([Altmann et al., 2006](#); [Canaan et al., 2009](#); [Dheekollu et](#)

74 [al., 2021](#); [Humme et al., 2003](#); [Lamontagne et al., 2021](#); [Lu et al., 2010](#); [Lupton and Levine, 1985](#);  
75 [Wood et al., 2007](#); [Yates et al., 1985](#)). EBNALP is another essential factor ([Mannick et al., 1991](#);  
76 [Szymula et al., 2018](#)) that initiates host cell proliferation alongside its co-activated target, EBNA2  
77 ([Alfieri et al., 1991](#); [Harada and Kieff, 1997](#); [Sinclair et al., 1994](#)), and interacts with several host  
78 proteins including TFs ([Han et al., 2001](#); [Ling et al., 2005](#); [Matsuda et al., 2003](#)). EBNA2 is likewise  
79 required for B cell immortalization ([Cohen et al., 1989](#)), notably through coordination with host  
80 TFs and their binding sites ([Lu et al., 2016](#); [Zhao et al., 2011](#)) and with EBNALP to drive early cell  
81 proliferation and viral LMP1 expression ([Peng et al., 2005](#)). The EBNA3 proteins (EBNA3A,  
82 EBNA3B, and EBNA3C) mediate a delicate balance of anti- and pro-oncogenic processes ([Allday  
83 et al., 2015](#); [Banerjee et al., 2014](#); [Parker et al., 1996](#); [Tomkinson et al., 1993](#); [White et al., 2010](#)).  
84 These include epigenetic repression of host tumor suppressor genes (*BIM*, *p14*, *p16*) and viral  
85 promoters ([Maruo et al., 2011](#); [Paschos et al., 2012](#); [Saha et al., 2015](#); [Skalska et al., 2010](#); [Styles  
86 et al., 2017](#)), competitive binding of the EBNA2-interacting host factor RBPJ ([Robertson et al.,  
87 1995](#); [Wang et al., 2015](#)), and inhibition of apoptosis ([Price et al., 2017](#)). Collectively, the EBNAs  
88 reshape the nuclear regulatory and transcriptional landscape of EBV<sup>+</sup> B cells, effectively hijacking  
89 B cell-intrinsic activation, expansion, and differentiation programs. Thus, EBV co-opts antigen-  
90 responsive host immune mechanisms for the ulterior purposes of viral replication and  
91 propagation.

92 While the EBNAs engage cell proliferation machinery at the epigenetic and transcriptional level  
93 in the nucleus, the LMPs (LMP1, LMP2A, and LMP2B) do so at the cell membrane by simulating  
94 antigen-induced signal transduction pathways. The essential LMP1 promotes B cell activation  
95 through mimicry of a constitutively active CD40 receptor ([Kilger et al., 1998](#); [Uchida et al., 1999](#))  
96 and interacts with Tumor Necrosis Factor (TNF) receptor-associated factors (TRAFs) to activate  
97 NF- $\kappa$ B pathway signaling via IKK ([Devergne et al., 1996](#); [Eliopoulos et al., 2003](#); [Greenfeld et al.,  
98 2015](#); [Luftig et al., 2003](#)). These interactions induce anti-apoptotic pathways, MHC-mediated  
99 immune recognition, pro-inflammatory responses, and cell migration. Downstream consequences  
100 include oncogenic proliferation and survival but also induction of pro-apoptotic responses  
101 ([Devergne et al., 1998](#); [Fries et al., 1999](#); [Greenfeld et al., 2015](#); [Henderson et al., 1991](#); [Shair et  
102 al., 2008](#); [Wang et al., 2017](#)). Thus, as in antigen-induced B cell activation (and subsequent  
103 differentiation), adept regulatory control of NF- $\kappa$ B signaling ([Hoffmann et al., 2002](#); [Mitchell et al.,  
104 2018](#); [O'Dea et al., 2007](#); [Roy et al., 2019](#)) is dispositive for the fate of a given EBV<sup>+</sup> B cell.  
105 Although it is not essential for transformation, LMP2A promotes cell survival through mimicry of a  
106 stimulated B cell receptor (BCR), which activates signaling cascades complementary to those  
107 induced by LMP1 ([Anderson and Longnecker, 2008](#); [Fish et al., 2020](#); [Guasparri et al., 2008](#);

108 [Portis and Longnecker, 2004](#)). LMP2A expression further predisposes EBV<sup>+</sup> B cells to survival by  
109 lowering antigen affinity selection thresholds *in vivo* ([Minamitani et al., 2015](#)). Thus, EBV latent  
110 membrane proteins play integral roles in B cell proliferation in the absence of antigen licensing  
111 and in avoiding replicative dead ends effected by antiviral sensing.

112 Clearly, key EBV gene products manipulate diverse host programs at early stages to achieve  
113 sustained latency ([Mrozek-Gorska et al., 2019](#); [Pich et al., 2019](#)). Many such perturbations involve  
114 extensive rewiring of epigenetic and transcriptional regulatory modules. EBV researchers have  
115 used methods such as RNA-, ATAC- (Assay for Transposase-Accessible Chromatin), and ChIP-  
116 seq (Chromatin Immunoprecipitation) to study these changes at various levels in the gene  
117 regulatory hierarchy within early infected cells and transformed lymphoblastoid cell lines (LCLs)  
118 ([Arvey et al., 2012](#); [Jiang et al., 2017](#); [McClellan et al., 2013](#); [Mrozek-Gorska et al., 2019](#); [Wang](#)  
119 [et al., 2019](#); [Zhou et al., 2015](#)). Recently, the epigenetic and transcriptional roles of EBNA1 were  
120 interrogated through time-resolved multi-omics ([Lamontagne et al., 2021](#)). While these and other  
121 studies provide indispensable insights regarding virus-induced genome-wide expression and  
122 regulation, they have relied on bulk ensemble sequencing. Such assays yield population-  
123 averaged measurements that obscure variation arising from intrinsic stochasticity ([Raj et al.,](#)  
124 [2006](#); [Raj et al., 2010](#); [Raj and Van Oudenaarden, 2008](#)), asynchronous behaviors, and  
125 heterogeneous cell subsets. Specifically, ensemble averaging fails to capture cell-matched  
126 measurements across genes, which precludes identification of coordinated expression programs  
127 or epigenomic regulatory patterns in specific phenotypes. By contrast, single-cell sequencing  
128 provides refined genome-wide views of expression and regulation that preserve the ability for the  
129 identification of heterogenous cell states with low bias ([Buenrostro et al., 2015](#); [Junker and van](#)  
130 [Oudenaarden, 2014](#); [Shalek et al., 2013](#); [Shapiro et al., 2013](#); [Wills et al., 2013](#)). Given the  
131 complexity of host-virus relationships, single-cell -omics approaches are essential to dissect the  
132 early stages of EBV infection and the distinct fate trajectories it comprises. We previously used  
133 single-cell RNA sequencing (scRNA-seq) to identify EBV-driven heterogeneity in LCLs ([SoRelle](#)  
134 [et al., 2021](#)). Recent advances in single-cell multimodal -omics methods have made it possible to  
135 integrate scRNA-seq with several levels of hierarchical regulation ([Efremova and Teichmann,](#)  
136 [2020](#)), which can provide greater insight into the mechanistic origins underlying gene expression.  
137 These include techniques for obtaining cell-matched measurements of mRNA transcripts,  
138 chromatin accessibility, and DNA methylation status ([Cao et al., 2018](#); [Chen et al., 2019](#); [Clark et](#)  
139 [al., 2018](#); [Zhu et al., 2019](#)), as well as other molecular levels. In this work, we leverage single-cell  
140 multiomics (scRNA-seq + scATAC-seq) to capture and explore the distinct gene expression and  
141 regulatory signatures that determine the course of EBV infection in primary human B lymphocytes.

142 **Results**

143

144 EBV asynchronously induces primary B cells into distinct phenotypic states early after infection

145 To interrogate chromatin accessibility and gene expression changes that occur upon EBV  
146 infection, we isolated primary human B cells from the peripheral blood of two donors and infected  
147 them with the B95-8 strain of EBV. Infections were performed at a multiplicity of infection (MOI)  
148 of 5 to ensure latent gene expression in every cell ([Nikitin et al., 2010](#)). We cryopreserved samples  
149 of infected cells at 2-, 5-, and 8-days post-infection in addition to uninfected cells (Day 0) from  
150 each donor sample following B cell enrichment. Cell samples from each donor and timepoint were  
151 simultaneously thawed, prepared to >90% viability, and processed into single-cell multiome  
152 libraries. Single-cell matched transcript and accessibility data were obtained through standard  
153 NGS, alignment, counting, and quality control (QC) methods (**Table S1**).

154 EBV infection induced broad transcriptomic changes in B lymphocytes at high efficiency, as  
155 evidenced by the near-complete loss of resting phenotypes (Day 0) within two days of infection.  
156 New states emerged between Day 2 and Day 5, while subtle shifts in state proportions defined  
157 the period between Day 5 and Day 8 (**Figure 1A**). Total and unique transcripts per cell increased,  
158 particularly between Day 0 and Day 2, while mitochondrial gene expression increased gradually  
159 (**Figure 1B**). Total transcript and mitochondrial distributions at Day 2 exhibited two modes, which  
160 was consistent with the presence of both non-proliferative and mitotic cells identified by S-phase  
161 and G2M-phase marker scoring (**Figure 1C**).

162 Unsupervised methods revealed subpopulations (clusters) in cell cycle-regressed aggregated  
163 scRNA-seq time courses. Two clusters corresponded to uninfected B cells (c3, c8); seven were  
164 post-infection B cell phenotypes (c0, c1, c2, c4, c5, c6, c7); and two were T cells (c9) and CD14<sup>+</sup>  
165 monocytes (c10) carried over from PBMCs despite extensive B-cell enrichment (**Figure 1D**).  
166 Genome-wide expression correlation was higher among post-infection states relative to  
167 uninfected cells, and certain phenotypes were more strongly correlated (e.g., c0 with c1; c4 with  
168 c7, **Figure 1E**). Sorting cluster membership by day yielded coarse-grained dynamics of cell state  
169 transitions (**Figure 1F**). We determined top differential genes in each cluster (one-vs-all-others)  
170 to inform state identity annotations (**Figure 1G**). Identified clusters included many genes known  
171 to be modulated in EBV infection and were broadly consistent across both donors with respect to  
172 top marker genes, cell population frequencies, and temporal emergence (**Figures S1-S4**).

173

174

175

176 Infected cell state heterogeneity is linked to antiviral and B cell-intrinsic responses

177 Cluster analysis deconvolved heterogeneous biological states within each sample and  
178 revealed phenotypes retained across multiple timepoints (**Figure 2**). At this resolution, we  
179 estimated time- and state-level trends in viral gene expression, variation in metabolic activity, and  
180 transcript diversity (**Figure 2A**). Overall, c0, c1, c2, c5, and c6 exhibited the highest levels of EBV  
181 transcripts and more unique transcripts than c3, c4, c7, and c8. Mitochondrial gene fraction and  
182 unique feature content were highest in c6 and lowest in c4 and c7, although c7 had a long-tailed  
183 distribution of mitochondrial expression (20-80%) prior to QC, indicative of (pre-) apoptotic cells.  
184 All clusters except uninfected B cells (c3, c8) displayed broad innate antiviral and interferon-  
185 stimulated gene (*ISG* and *IFI* member) expression. Antiviral gene expression was generally higher  
186 and exhibited greater variance in c7 than c4 and persisted at roughly uniform levels in c0, c1, c2,  
187 c5, and c6 (**Figure 2B**). Through joint consideration of cluster-resolved expression trends for viral,  
188 mitochondrial, and interferon-stimulated genes, we distinguished uninfected cells (c3, c8) and two  
189 classes of cells with the hallmarks of antiviral response: those with low proliferation and negligible  
190 viral expression (c4, c7) and those with viral and metabolic indicators of progressive EBV infection  
191 (c0, c1, c2, c5, c6).

192 Next, we extensively analyzed differentially expressed genes (DEGs) among clusters and  
193 groups, including pairwise comparisons of all post-infection phenotypes (**Figures 2C, S5-S11**).  
194 The two resting cell phenotypes differed in their expression of *IGHD*, *IGHM*, *CD27*, and other  
195 markers that distinguish naïve (c8) from memory (c3) B cells. In addition to interferon response  
196 signatures, non-proliferating infected cells exhibited an overall reduction in gene expression and  
197 upregulated stress response markers. These included the highest overall expression of actin  
198 sequestration genes (*TMSB10*, *TMSB4X*) and, particularly within c7, numerous ribosomal subunit  
199 genes (e.g., *RPS27A*). Cells in c4 were distinguished by elevated expression of *MARCH1*, which  
200 encodes an E3 ubiquitin ligase that regulates the type I interferon response ([Wu et al., 2020](#)).  
201 Unlike c4, c7 cells also contained high transcript levels for genes involved in oxidative stress  
202 (*TXN*, *FTL*, *FTH1*), cytochrome oxidase subunits (e.g., *COX7C*), ubiquitin genes (*UBA52*, *UBL5*)  
203 and highly variable mitochondrial fractions. Among EBV<sup>+</sup> cells with hallmarks of elevated  
204 respiration, those in c6 were most clearly consistent with proliferating cells based on upregulated  
205 cell cycle markers. Cells in c0 were distinguished by upregulation of *FCRL5* and *LY86-AS1*, an  
206 antisense RNA to a lymphocyte antigen (*LY86*) that mediates innate immune responses. Cells in  
207 this cluster also displayed markers consistent with the early stages of pre- germinal center  
208 activated B cells (e.g., *CCR6*, *CD69*, *POU2AF1*, *TNFRSF13B*, *PIK3AP1*). Notably, cells in c1 and  
209 c2 contained the highest levels of the EBV gene *BHRF1*. Between these two phenotypes, c2 was

210 enriched for genes involved in NF- $\kappa$ B signaling and known markers of EBV-mediated B cell  
211 activation (*NFKBIA*, *TNFAIP3*, *EBI3*) while c1 appeared to be derived from naïve cells (based on  
212 *IGHD* and other carryover genes) and exhibited near-unique expression of *SH3RF3/POSH2* and  
213 *FIRRE*, a MYC-regulated long non-coding RNA (lncRNA). Finally, c5 displayed upregulation of  
214 immunoglobulin heavy and light chains (*IGHA1*, *IGHG1*, *IGHM*, *IGKC*, *IGLC1-3*) as well as genes  
215 involved in B cell differentiation (*MZB1*, *PRDM1/BLIMP1*, *XBP1*). Gene ontology (GO) networks  
216 were also generated for top DEGs from one-versus-all-other comparisons to facilitate phenotype  
217 annotations (**Figures S12-S16**).

218

219 A map of B cell phenotypes and fate trajectories in early EBV infection

220 Graph-based pseudotime ([Qiu et al., 2017](#)) approximated EBV-induced state transitions when  
221 anchored from resting cells (**Figure 3A**). Pseudotime scoring was used to track state dynamics  
222 of the top 25 marker genes for each phenotype and four example expression trajectories are  
223 highlighted (**Figure 3B**). Collectively, flow cytometry for the B cell marker CD19 and CD23  
224 (upregulated in EBV infection) at each timepoint (**Figure S17**), cluster-specific DEGs, network  
225 ontologies, and pseudotime led us to propose a multi-phenotype model for heterogeneous cell  
226 fate trajectories (**Figures 3C, S18-S19**) that manifest in early EBV infection *in vitro*. In this model,  
227 naïve (c8) and memory (c3) B cells infected with EBV either undergo antiviral response-mediated  
228 arrest (c4) or EBV-driven hyperproliferation (c6) within several days of infection.  
229 Hyperproliferating cells can subsequently enter one of several activated states (c0, c1, c2) or  
230 undergo growth arrest (c7). Further, differentiated B cells (c5) can develop following activation in  
231 a manner analogous to effector cell exit from the germinal center reaction.

232 Among activated phenotypes, c2 matched classical EBV-mediated activation of NF- $\kappa$ B  
233 pathway genes, apoptotic regulators, and other known biomarkers ([Cahir-McFarland et al., 2004](#);  
234 [Messinger et al., 2019](#)). Cells in c1 were consistent with a related activation intermediate that  
235 originated from EBV<sup>+</sup> naïve cells. Despite the relatively short timecourse, c2 and c5 began to  
236 reflect the continuum of activation and differentiation phenotypes we previously characterized in  
237 LCLs ([SoRelle et al., 2021](#)), which are considered to be immortalized at 21-28 days post-infection  
238 ([Nilsson et al., 1971](#)). We confirmed these similarities by merging Day 8 and the LCL GM12878,  
239 for which scRNA-seq data was previously reported and analyzed ([Osorio et al., 2019](#); [Osorio et](#)  
240 [al., 2020](#); [SoRelle et al., 2021](#)) (**Figure S20**). Conceivably, EBV<sup>+</sup> cells could also transition to a  
241 plasmablast phenotype (c5) from memory cells (c3) through hyperproliferation (c6) via division-  
242 linked differentiation ([Hodgkin et al., 1996](#)), effectively bypassing intermediate states.

243 Conversely, cells in c7 highlighted diverse origins of EBV<sup>+</sup> cell growth arrest, apoptosis, and  
244 senescence, which each provide host defenses against oncogenic malignancies ([Bartkova et al.,](#)  
245 [2006](#); [Nikitin et al., 2010](#)). In addition to highly variable mitochondrial expression and the lowest  
246 transcript levels of any state, this phenotype was defined by broad upregulation of genes involved  
247 in ribosome biogenesis-mediated senescence (*RPS14*, *RPL29*, *RPS11*, *RPL5*) ([Lessard et al.,](#)  
248 [2018](#); [Nishimura et al., 2015](#)) and stress-associated sequestration of actin monomers that favor  
249 G-actin formation (*TMSB4X*, *TMSB10*, *PFN1*) ([Kwak et al., 2004](#)). A subset of cells within c7 also  
250 contained elevated levels of cell cycle markers (*MKI67*, *TOP2A*, *CCNB1*, *CENPF*) carried over  
251 from pre-arrest hyperproliferation (**Figure S21**).

252

253 **Evidence for EBV induction of an activated precursor to early memory B cells (AP-eMBC)**

254 We next sought to compare early infected phenotypes from our multistate model with cells  
255 isolated from secondary lymphoid organs. We acquired single-cell RNA-seq data from human  
256 tonsil tissue and identified germinal center (GC) cell subsets (**Figure 4A**), which we analyzed  
257 alongside early infection phenotypes of interest. EBV<sup>+</sup> NF-κB activated cells (c2) clearly mimicked  
258 GC light zone (LZ) B cells; *MKI67<sup>hi</sup>* cells (c6) matched actively cycling cells (including GC dark  
259 zone (DZ) B cells); and EBV<sup>+</sup> differentiated cells (c5) matched plasmablasts and plasma cells (PB  
260 / PC). Cells in c0 were most like pre-GC naïve and memory B cell (MBC) subsets (**Figure 4B-D**).  
261 Further, numerous c0 markers were consistent with both pre-GC activated B cells (*SELL*, *BANK1*,  
262 *CD69*, *GPR183* (*EBI2*)) and memory B cell phenotypes (*SELL*, *BANK1*, *GPR183*, *PLAC8*)  
263 recently identified from scRNA-seq of tonsils in response to antigen challenge ([King et al., 2021](#))  
264 (**Figure 4C-D**). Cells in c0 further exhibited upregulation of genes with essential roles in B cell  
265 activation (*TNFRSF13B/TAC1*) ([Wu et al., 2000](#)) and germinal center formation (*POU2AF1/OCA-*  
266 *B*) ([Kim et al., 1996](#); [Luo and Roeder, 1995](#); [Schubart et al., 1996](#)) (**Figure S18**). Moreover, c0  
267 displayed elevated *CCR6*, a marker of an activated precursor (AP) state that can generate early  
268 memory B cells (eMBCs) ([Glaros et al., 2021](#); [Suan et al., 2017](#)) (**Figure 5A**).

269 We subsequently validated the generation of CCR6<sup>+</sup> AP-eMBC B cells in response to EBV  
270 infection through time-resolved FACS (**Figures 5B-D, S22-S24**). Resting B cells were CCR6<sup>lo</sup>  
271 and remained so until between 2 and 5 days after infection. Further, we observed that the most  
272 proliferative cell fraction at day 8 was CCR6<sup>lo</sup> and a moderately proliferative cell population was  
273 CCR6<sup>hi</sup>. While the most proliferative cells were CCR6<sup>lo</sup>/CD23<sup>lo</sup>, the proliferative CCR6<sup>hi</sup> cells  
274 displayed variable CD23 levels (**Figure 5B**). Consistent with our scRNA time course,  
275 CCR6<sup>hi</sup>/CD23<sup>hi</sup> and CCR6<sup>hi</sup>/CD23<sup>lo</sup> populations respectively corresponded to c1/c2 and c0 and  
276 emerged within 5 days (**Figure 5C**). Based on CD27 and IgD status, these populations

277 predominantly originated from naïve or non-switched memory versus switched memory cells,  
278 respectively; notably, cells from these different resting phenotypes were present in each  
279 population gated by CCR6 and CD23 status (**Figure 5D, S24C**). Rapidly proliferative  
280 CCR6<sup>lo</sup>/CD23<sup>lo</sup>/CD27<sup>hi</sup>/IgD<sup>lo</sup> cells were consistent with infected memory B cells transitioning to  
281 plasmablasts ( $c3 \rightarrow c6 \rightarrow c5$  model trajectory; ~72% of CCR6<sup>lo</sup>/CD23<sup>lo</sup> cells). Marginally less  
282 proliferative CCR6<sup>hi</sup>/CD23<sup>lo</sup>/CD27<sup>hi</sup>/IgD<sup>lo</sup> cells were consistent with stimulated AP-eMBCs  
283 ( $c3 \rightarrow c6 \rightarrow c0$  model trajectory; ~74% of CCR6<sup>hi</sup>/CD23<sup>lo</sup> cells). We also observed an IgD<sup>hi</sup> naïve  
284 population that matched the pre-GC AP-eMBC phenotype ( $c8 \rightarrow c6 \rightarrow c0$ ; (~25% of CCR6<sup>hi</sup>/CD23<sup>lo</sup>  
285 cells). Finally, an even less proliferative CCR6<sup>hi</sup>/CD23<sup>hi</sup>/IgD<sup>hi</sup> population matched activated naïve  
286 (or non-switched memory) cells destined for GC BC ( $c8 \rightarrow c6/c0 \rightarrow c1/c2$ ; ~80% of CCR6<sup>hi</sup>/CD23<sup>hi</sup>  
287 cells) and the minor subset (~17%) of CCR6<sup>hi</sup>/CD23<sup>hi</sup> cells that was IgD<sup>lo</sup> was consistent with  
288 MBCs induced by EBV to undergo a pseudo-GC reaction ( $c3 \rightarrow c6/c0 \rightarrow c2$ ) (**Figure 5C-E**).  
289 Intriguingly, a subset of CCR6<sup>+</sup> cells displaying the AP phenotype apparently persists long after  
290 the early stages of infection based on scRNA-seq data from LCLs (**Figure S25**). Thus, c0 in our  
291 model matches a virus-induced common progenitor state from which PBs, GC BCs, and early  
292 MBCs have been shown to originate in response to antigen stimulation ([Taylor et al., 2015](#)). Our  
293 results further indicate that both naïve and memory B cells can achieve this multipotent state at  
294 different frequencies upon *in vitro* infection and that the AP-eMBC phenotype is perpetuated in  
295 EBV-immortalized B cells.

296

#### 297 Linked expression and accessibility illuminate regulatory mechanisms in phenotype trajectories

298 We next investigated potential regulatory mechanisms underlying DEGs observed across  
299 phenotypes. Expression data were jointly analyzed with cell-matched measurements from single-  
300 cell Assay for Transposase-Accessible Chromatin sequencing (scATAC-seq) and annotated by  
301 state (**Figures 6A-B, S26A-B**). While total and unique transcripts per cell increased through early  
302 infection, global chromatin accessibility decreased substantially upon infection. Resting (c3, c8)  
303 and hyperproliferative (c6) cells had the highest overall accessibility. There were significantly  
304 more peaks in the NF- $\kappa$ B activation state (c2) relative to other activation intermediates (c0 and  
305 c1; two-tailed t-test,  $p < 2.2 \times 10^{-16}$  and  $1.4 \times 10^{-14}$ , respectively) and differentiated cells (c5;  $p <$   
306  $2.2 \times 10^{-16}$ ). Similar accessibility reduction occurred in both donors in the first five days, with  
307 increased accessibility recovered between Day 5 and Day 8 (including to higher than resting  
308 levels in one donor) (**Figures 6B, S27**). This indicated that EBV-induced heterochromatinization  
309 is likely transient in successfully infected cells (i.e., those that evade innate- and damage-  
310 mediated arrest).

311 We found 954 linked feature genes derived from the top 100 marker genes for each cluster  
312 using the multimodal integration capabilities of the Signac package in R ([Stuart et al., 2021](#)). Of  
313 these 954 genes, 177 were significant DEGs with linkages to 476 differentially accessible peaks  
314 (DAPs). This translated to 18.6% of tested genes with potential DAP-linked regulation (**Figures**  
315 **6C, S26C-D**). We identified genes linked (in *cis*) to DAPs to explore phenotype-associated gene  
316 regulatory relationships (**Figure S28A**). Joint analysis of DAP-linked DEGs yielded four regulatory  
317 patterns: higher accessibility with higher expression (+/+); lower accessibility with higher  
318 expression (-/+); lower accessibility with lower expression (-/-); and higher accessibility with lower  
319 expression (+/-). (**Figure S28B**). The +/+ and -/- patterns were characteristic of positive regulatory  
320 sites. The less frequently observed -/+ and +/- patterns were consistent with closure or opening  
321 of ATAC sites with negative regulatory functions, respectively. Analysis of genes of interest  
322 including *CCR7*, *CXCR4*, *RUNX3*, *BACH2*, *JCHAIN*, and *PRDM1* provided examples of each  
323 regulatory pattern and their variation among states (**Figures S28C, S29-S30**).

324 We developed joint scRNA + scATAC profiles for major infection fate trajectories in our model  
325 (**Figure 6C-F**). The path from resting cells to EBV<sup>+</sup> arrested/senescent cells (c38 → c47) was  
326 characterized by global reductions in accessibility and expression. 34.3% of all DEGs between  
327 resting cells and these non-proliferative EBV<sup>+</sup> fates were linked to DAPs that become inaccessible  
328 after infection (c38/c47 peaks). Top DAP-linked DEGs in innate arrested cells (c4) corresponded  
329 to upregulation of interferon-responsive genes and downregulation of mitochondrial genes, while  
330 stress- and damage-induced senescent cells (c7) were distinguished by their high expression of  
331 interferon-stimulated genes (e.g., *ISG15*) and ribosomal transcripts (e.g., *RPS14*). Cells in each  
332 of these clusters also displayed reduced expression of the proto-oncogenic tyrosine kinase gene  
333 *LYN* linked to closure of multiple regulatory sites following infection (**Figure 6D**).

334 The reduction in ATAC peaks within c7 was consistent with the formation of senescence-  
335 associated heterochromatin foci (SAHF) ([Courtois-Cox et al., 2008](#); [Di Micco et al., 2011](#); [Lenain](#)  
336 [et al., 2017](#)) (**Figure S31**). Because senescence can arise from diverse mechanisms such as  
337 innate immune sensing or growth-induced DNA damage, we used higher resolution clustering to  
338 reveal c7 subsets (7a and 7b). These subsets displayed DEGs involved in the cell cycle and  
339 antiviral sensing (**Figure S32**). Different *HMGB2* levels between 7a and 7b were notable, as this  
340 gene's product mediates diverse roles in sensing ([Yanai et al., 2009](#)), double-stranded break  
341 repair ([Krynetskaia et al., 2009](#)), and p53 downregulation ([Stros et al., 2002](#)). Relative to resting  
342 B cells, *HMGB2* expression was strongly elevated in 7b (as in the hyperproliferative state, c6) but  
343 only mildly so in 7a (similar to c4, which could precede senescence ([Glück et al., 2017](#))). Similarly,  
344 cell cycle markers were lower in 7a than 7b. Thus, 7a was consistent with EBV<sup>+</sup> cells that arrest

345 almost immediately via innate sensing and become senescent, whereas 7b matched a trajectory  
346 in which EBV<sup>+</sup> hyperproliferative cells become senescent following replicative stress response  
347 induction. Notably, both 7a and 7b exhibited elevated levels of ribosomal subunit mRNAs (**Figure**  
348 **S32C-D**).

349 NF- $\kappa$ B activated EBV<sup>+</sup> cells (c2) exhibited loss of accessibility at 1,142 sites present within  
350 resting cells in both donors (8.7% of all resting cell peaks). This reduction paralleled upregulated  
351 expression of the polycomb group repressor *EZH2* and a polycomb-interacting methyltransferase,  
352 *DNMT1* (**Figure S33**). However, EBV-activated cells possessed 668 peaks absent in resting cells  
353 (c2!c38) that were linked to 595 unique genes. 154 of these (25.9%) were DEGs between resting  
354 and activated cells (**Figure 6E**). These 154 c2!c38 DAP-linked DEGs included 109 upregulated  
355 and 45 downregulated genes from c38 $\rightarrow$ c2. Upregulated genes included regulators of apoptosis  
356 and tumor suppression (*BCL2A1*, *TNFRSF8*, *PDCD1LG2*, *ST7*, *IQGAP2*, *TOPBP1*, *CD86*);  
357 proliferation (*CDC47*, *MKI67*); B cell signaling (*NFKBIA*, *MAPK6*, *TNIP1*, *TRAF3*); inflammation  
358 (*SLC7A11*, *RXRA*, *ZC3H12C*); oxidative stress (*SLC15A4*, *TXN*); and epigenetic remodeling  
359 (*AHRR*, *NCOR2*). The 45 downregulated c2!c38 DAP-linked DEGs included *CCR7*,  
360 acetyltransferases (*EPC1*, *KAT6B*), apoptotic and stress response regulators (*STK39*,  
361 *STK17A/DRAK1*, *VOPP1*, *ZDHHC14*), negative regulators of B cell signaling (*CBLB*), and the  
362 tumor suppressor *ARRDC3* (**Figure S34**).

363 In a third example, we explored DAP-linked DEGs between EBV-induced activated (c2) and  
364 differentiated (c5) phenotypes. Activated cells exhibited 999 called peaks that were absent in  
365 differentiated cells (c2!c5 DAPs) while only 13 new peaks emerged in differentiated cells (c5!c2  
366 DAPs) in both donors. This corresponded to a 15% net reduction in accessible peaks in the  
367 c2 $\rightarrow$ c5 transition. Notably, c2!c5 DAPs found in both donors were linked to 13.4% of all DEGs  
368 identified between these states in the scRNA assay. Key c2 $\rightarrow$ c5 DAP-linked DEG dynamics  
369 included downregulation of NF- $\kappa$ B family genes and upregulation of plasmablast-specific  
370 transcriptional regulators, translation factors, and protein export machinery (i.e., facilitators of Ig  
371 synthesis, secretion, and protein folding chaperones) (**Figures 6F, S10**).

372 By mapping multiome reads to a concatenated reference (human + EBV), we were able to  
373 detect increased accessibility within the EBV genome over time after infection. We detected 21  
374 unique viral ATAC peaks (20 of 21 common to both donors) including at TSSs for essential viral  
375 genes such as the *EBNAs* and *LMP1* (**Figure S35**). Quantification of episome peak-containing  
376 cells by phenotype revealed that EBV<sup>+</sup> activated and hyperproliferative cells had the greatest  
377 number of accessible loci relative to other post-infection phenotypes. These sites included the C  
378 promoter (Cp) for *EBNA1*, *EBNA2*, and *EBNA3A-C*; the *LMP1* TSS; the TSS for *BMRF1*, a DNA

379 polymerase accessory protein; and the *BHLF1* locus, which was recently recognized as a  
380 facilitator of latency and B cell immortalization ([Yetming et al., 2020](#)) (**Figure S36A-B**). Innate  
381 arrested cells (c4) exhibited the lowest frequency of cells with accessible episomal loci, followed  
382 by growth-arrested cells (c7) (**Figure S36C**).  
383

#### 384 Post-infection cell fates exhibit differential enrichment of TF motifs

385 To further investigate regulatory differences by phenotype, we assayed TF binding motif  
386 enrichment by state (**Figure S37**). We identified variable motif enrichment linked to resting cell  
387 phenotypes and among non-arrested post-infection states (**Figure S37A**). Variation in accessible  
388 motifs broadly aligned with phenotypic gene expression with respect to antiviral response  
389 induction, promotion of cell growth, and oncogenesis (**Figure S37B-C**). Activated B cell (c2)  
390 ATAC peaks were enriched in binding sites for proto-oncogenic TFs including members of the  
391 REL (cREL, RelA, RelB), AP-1 (FOS, FOSB, JUNB, JUND), and EGR (EGR1-4) families.  
392 Enhanced accessibility at NF- $\kappa$ B family binding sites within activated cells was noteworthy, given  
393 the observed concurrent upregulation of NF- $\kappa$ B pathway gene expression. Similar phenotypic  
394 consistency was observed within differentiated cells (c5), which were enriched in accessible  
395 motifs for IRF4, IRF8, and XBP1. Globally, both resting B cell phenotypes and the innate sensing  
396 arrest state shared the greatest motif correlation with each other ( $R>0.75$ ) and the lowest  
397 correlation with EBV-activated and hyperproliferating cells ( $0.55<R<0.7$ ) (**Figure S38**).  
398

#### 399 An informatics pipeline to infer phenotype-resolved TF signatures and gene regulatory elements

400 The prevalence of DAPs linked to DEGs known to be modulated in *trans* by EBV gene products  
401 led us to interrogate phenotype-specific TF signatures genome-wide. To do so, we employed a  
402 bioinformatic workflow to obtain ChIP-seq referenced inferences of single-cell phenotypes from  
403 scATAC data, which we termed “crisp-ATAC” (**Figures S39, S40**). We expected that ensemble-  
404 averaged ChIP data from an appropriate reference cell type would contain TF binding (and  
405 epigenetic) data from a superposition of cell phenotypes at high coverage, thus maximizing  
406 chances to identify overlaps with comparatively sparse scATAC cluster data. We further reasoned  
407 that phenotypic variation in TF binding site accessibility would have biological consequences.

408 We sought to predict viral EBNA and LMP1-mediated NF- $\kappa$ B accessible sites at promoters,  
409 enhancers, and actively transcribed genes in each state of our model. To do so, we applied crisp-  
410 ATAC recipes to intersect peaks from each scATAC phenotype with ChIP-seq peaks for viral  
411 EBNA, NF- $\kappa$ B/Rel TFs, H3K4me1, H3K4me3, H3K27ac, H3K36me3, and RNA Pol II ([Jiang and](#)  
412 [Mortazavi, 2018](#)) (**Figure S39C**). Hyperproliferative cells (c6), EBV-activated cells (c2), and

413 resting memory B cells (c3) exhibited up to 3-fold more enhancers and promoters at known  
414 EBNA2 binding sites relative to naïve B cells (c8), other activation intermediates (c0, c1),  
415 plasmablasts (c5), arrested states (c4, c7), and non-B cells (c9, c10). Similar patterns were found  
416 for EBNA3C and EBNALP sites (**Figure S39C**, left column) as well as Rel family TF binding sites  
417 (cRel, RelA, and RelB). Enhancers, promoters, and actively transcribed genes were consistently  
418 enriched in c2, c3, and c6 and depleted in c4 and c7, with intermediate levels present in c0, c1,  
419 c5, and c8. By accounting for peaks conserved in both biological replicates, we demonstrated  
420 low-noise measurements of DAPs for use with crisp-ATAC and characterized DAP frequencies  
421 and interval length distributions across all pairwise phenotype comparisons (**Figure S40**).  
422

#### 423 crisp-ATAC finds TF-linked expression signatures that vary across distinct EBV<sup>+</sup> cell fates

424 We applied crisp-ATAC to capture regulatory variation among infection phenotypes with  
425 respect to key viral transcriptional co-activators. We first compared the innate sensing arrest (c4)  
426 and NF- $\kappa$ B (c2) states (**Figure 7A**), as these represent starkly different post-infection fates. Peak  
427 data were extracted and gated to obtain c2/c4 DAPs present in both donors (n=1,873), which  
428 yielded linked gene predictions (n=1,514) (**Figure 7B-C**). The c2/c4 linked gene ontology network  
429 was enriched for innate defense (inflammation, antimicrobial processes) and EBV-induced  
430 responses (lymphocyte activation, regulation of apoptosis) (**Figure 7D**). Taking a macroscopic  
431 view, we found that predicted c2/c4 linked genes included 42.5% (71 of 167) of known EBV super-  
432 enhancer (EBVSE) site-linked genes ([Zhou et al., 2015](#)). Consequently, 41-55% of EBNA-  
433 associated c2/c4 DAPs also overlapped a peak for the super-enhancer-associated host TF RelA.  
434 Of the 71 EBVSE-linked genes identified for c2/c4, 19 (27%) were linked to EBNALP ChIP-seq  
435 peaks; 22 (31%) to EBNA2 ChIP-seq peaks; and 15 (21%) to EBNA3C ChIP-seq peaks. EBVSE-  
436 linked genes were enriched in EBNA-associated DAP-linked DEGs relative to size-matched  
437 random samples of genes in the captured transcriptome (**Figure 7E**).

438 We analyzed specific genes of interest based on 1) EBVSE membership, 2) GO process  
439 involvement, and/or 3) empirically demonstrated importance to EBV infection. The NF- $\kappa$ B  
440 activated gene and signal transducer *TRAF1*, whose gene product interacts with viral LMP1, was  
441 identified through all three of these routes ([Devergne et al., 1996](#); [Eliopoulos et al., 2003](#); [Fries et](#)  
442 [al., 1999](#); [Greenfeld et al., 2015](#); [Sandberg et al., 1997](#)). We found c2/c4 DAPs associated with  
443 one or more EBNA at -3kb, +2kb, and +37kb relative to the *TRAF1* TSS, each with significant  
444 positive correlation to *TRAF1* expression (p<0.05 for correlation z-score). Notably, these EBNA-  
445 associated regulatory loci exhibited reduced accessibility in stress arrest (c7), activation  
446 intermediate (c1) and differentiated (c5) states compared with c2 (**Figure 7F**).

447 We used a grouped crisp-ATAC comparison (*c256/c38*) to study changes associated with the  
448 trajectory for successful EBV-induced B cell immortalization (**Figure S41**). We analyzed viral co-  
449 activator-associated DAPs between proliferative (c6) and LCL-like phenotypes (c2, c5) versus  
450 resting B cells (c3, c8). Despite the net reduction in accessibility after infection, we identified 245  
451 unique genes linked to 1,824 peaks present in all tested EBV<sup>+</sup> states (*c256*) but absent in both  
452 resting phenotypes (*c38*) (**Figure S41A-C**). 166 of the 245 genes were linked to a binding site for  
453 at least one EBNA, and 18 of these genes overlapped with EBVSE targets (7.3% of predicted  
454 genes, 10.8% of known EBVSE genes). Only 31 GO process terms were shared across the top  
455 100 terms for each tested EBNA, accounting for 15% of unique terms (**Figure S41D**). We selected  
456 the *c256/c38* EBNA targets *TNFRSF8* (CD30), *CD274* (PD-L1), and *PDCDL1G2* (PD-L2) based  
457 on their therapeutic relevance to EBV-associated lymphomas. For each gene, we confirmed the  
458 presence of EBNA-associated DAP-linked DEGs by phenotype. These included three  
459 *EBNA2*<sub>*c256/c38*</sub> sites near the *TNFRSF8* TSS (-17kb, -12kb, and +16kb) and a shared multi-EBNA  
460 site -17kb from the *PDCDL1G2* TSS and +43kb from the end of the *CD274* gene (**Figure S41E**).  
461 These loci were enriched for Rel sites and activating histone marks in LCL reference data.

462 In a final example, we evaluated activated versus differentiated EBV<sup>+</sup> phenotypes (*c2/c5*) sites  
463 with known viral transcriptional co-activator binding in both donors to explore regulatory  
464 relationships that distinguished the phenotypes present in LCLs ([SoRelle et al., 2021](#)) (**Figure**  
465 **S42A**). 519 of 999 identified *c2/c5* peaks intersected with at least one EBNA binding site, from  
466 which 247 unique genes were predicted. 29 of 110 *c2/c5* EBNA2 site-linked genes (26.3%) were  
467 *c2/c5* DEGs in the scRNA assay, as were 34 of 115 *c2/c5* EBNALP site-linked genes (29.6%)  
468 and 20 of 125 *c2/c5* EBNA3C site-linked genes (16.0%). 20 site-linked genes were identified  
469 from all three viral co-activator recipes (**Figure S42B**), including the EBVSE-linked G protein  
470 coupled receptor *GPR137B*, a lysosomal transmembrane receptor that regulates mTORC1 activity  
471 and autophagy ([Gan et al., 2019](#); [Gao et al., 2012](#)). *GPR137B* was also identified as a *c2/c38*  
472 DAP-linked DEG, indicating inaccessible regulatory loci within resting cells as well. We identified  
473 two regulatory DAPs with significant positive correlation to gene expression at +14kb and +18kb  
474 relative to the *GPR137B* TSS. One of these sites (+14kb) coincided with EBNALP and EBNA3C  
475 binding sites but did not exhibit a *c2/c5* DAP. However, the second site (+18kb) overlapped with  
476 all three intersected EBNAAs and was a *c2/c5* DAP. Both sites also intersected with Rel family TFs  
477 (cRel, RelA, and RelB) (**Figure S42C**). Other genes involved in lysosome-mediated processes  
478 including autophagy and antigen presentation regulation were also identified from the *c2/c5*  
479 comparison (*TFEB*, *LAMP3*), albeit with modestly elevated but significant differential expression  
480 ([Martina et al., 2012](#); [Nagelkerke et al., 2014](#); [Settembre et al., 2011](#)). We also found numerous

481 other genes involved in immune activation signaling, apoptosis, and transcriptional regulation that  
482 displayed EBNA-associated *c2/c5* DAP-linked DEGs (**Figure S42D-E**). Collectively, these  
483 vignettes of post-infection cell trajectories highlight the genome-wide dynamics of diverse EBV-  
484 induced B cell responses captured within the single-cell multiomics dataset.

485

486 Single-cell imputation reveals transcriptomic dynamics of EBV infection of FCRL4<sup>+</sup>/TBX21<sup>+</sup> B cells

487 The EBV early infection model presented herein captures robust B cell phenotypes, each of  
488 which are exhibited by >1000 cells in the assay. However, we did not preclude the possibility that  
489 distinct rare populations of B cells may also be represented within the dataset. To explore this  
490 possibility with sufficient sensitivity, we implemented a recently reported method that minimizes  
491 technical read noise from transcript dropout in scRNA data ([Linderman et al., 2022](#)). Briefly, this  
492 method (ALRA) adaptively thresholds a low-rank approximation of the single-cell expression  
493 matrix in order to preserve biological zeros (true negatives) for gene expression and impute  
494 probable values in place of technical zeros (false negatives from dropout). Unsupervised  
495 clustering of ALRA-imputed data from Day 5 of the early infection timecourse revealed a small  
496 (1.5% of cells) yet distinctive population of B cells (**Figure 8A**). Notably, this subset expressed  
497 *FCRL4*, which encodes an inhibitory receptor that blocks BCR signaling ([Davis, 2007](#); [Sohn et](#)  
498 [al., 2011](#)); *TBX21* / *T-bet*, a gene for a canonical Th1 subset homeobox TF ([Szabo et al., 2000](#))  
499 that is also essential to an unconventional memory B cell subset ([Johnson et al., 2020](#); [Rubtsova](#)  
500 [et al., 2013](#); [Wang et al., 2012](#)); and *CXCR3*, which encodes a chemokine receptor that mediates  
501 migration in a subset of MBCs ([Muehlinghaus et al., 2005](#)). While these *FCRL4<sup>+</sup>* / *TBX21<sup>+</sup>* /  
502 *CXCR3<sup>+</sup>* cells displayed robust expression of lineage markers (e.g., *CD19*, *MS4A1/CD20*) and  
503 genes involved in the early stages of B cell activation (e.g., *CCR6*, *CD69*), they notably lacked  
504 expression of GC reaction gene signatures or plasmablast differentiation (**Figure 8B**). Rather, the  
505 most prominent feature of this population was broad upregulation of *FCRL* family genes including  
506 *FCRL5* and *FCRL6*, which was originally found to be expressed on NK and T cells ([Wilson et al.,](#)  
507 [2007](#)) but has recently been identified in B cell progenitors ([Honjo et al., 2020](#)). While these cells  
508 expressed markers of double-negative (DN & DN2) B cell populations (*TBX21*, *ITGAX*, *CXCR3*),  
509 such cells are typically *FCRL4<sup>-</sup>* ([Jenks et al., 2018](#); [Scharer et al., 2019](#)). This population was  
510 most consistent with Tissue-Like Memory (TLM) B cells based on the expression of the markers  
511 discussed above in addition to being *CD21<sup>-</sup>* / *FCRL5<sup>+</sup>* / *SOX5<sup>+</sup>* / *RTN4R<sup>+</sup>*, although differential  
512 *FCRL4* expression in TLM B cells has been reported ([Li et al., 2016](#); [Rakhmanov et al., 2009](#)).  
513 Top markers of the *FCRL4<sup>+</sup>* TLM-like phenotype in our dataset were also enriched for genes with  
514 roles mediating innate immunity and inflammatory responses; proto-oncogenes including *FGR*,

515 which has been shown to be induced by EBNA2 during EBV infection ([Cheah et al., 1986](#);  
516 [Knutson, 1990](#)); and an array of genes whose overexpression contributes to cell migration,  
517 metastasis, plasticity, and the potential for self-renewal in a variety of cell types.

518 We confirmed the presence of a Day 0 (EBV<sup>-</sup>) precursor to the Day 5 TLM phenotype, and we  
519 focused on this Day 0 TLM B cell cluster to assess pre- and post-infection differential gene  
520 expression (**Figure 8C**). Although TLM B cells were *FCRL4*<sup>+</sup> at Day 0, the expression of *FCRL4*  
521 increased following infection, consistent with our prior finding that *FCRL4* is a host biomarker of  
522 the EBV Latency IIb program ([Messinger et al., 2019](#)). *CCR6* expression in these cells increased  
523 following infection, indicating early B cell activation. However, key NF- $\kappa$ B pathway genes  
524 associated with subsequent GC B cell activation events were downregulated after infection in  
525 TLM B cells. Although upregulation of genes in this canonical pro-survival pathway was not  
526 observed, we found evidence for a *PAX5* / *FOXP4-AS1* / *FOXP4* axis, which has been reported  
527 to promote proliferation and anti-apoptotic signaling (**Figure 8D, violin plots**) ([Wu et al., 2019](#)).  
528 Critically, we observed EBV latent transcripts within TLM B cells at Day 5 and Day 8 in addition  
529 to upregulation of numerous genes with roles in cellular plasticity, tumorigenesis, migration, and  
530 self-renewal (**Figure 8D, dot plot**). In addition to *FCRL4*, *TBX21*, *CXCR3*, *ITGAX/CD11c*, and  
531 *FCRL5*, an unexpected set of genes known to mediate neural development, adhesion, and  
532 signaling were conserved and/or upregulated markers of this cell subset during the early infection  
533 timecourse (**Figures 8E, S43-S44**). These genes included *NRCAM*, *DPF3*, *PPP1R17*, *PCDH1*,  
534 *GABRA4*, and *GRID1*, which were identified through GO Process enrichment within TLM-like B  
535 cells (GO:0007399, FDR = 0.0075, 62 genes and GO:0035239, FDR = 0.035, 23 genes). Notably,  
536 several of these were also observable in subsets within the GM12878 LCL. Many of these and  
537 other genes upregulated within *FCRL4*<sup>+</sup> TLM-like B cells following EBV infection were also found  
538 in GM12878, which was derived from an independent biological donor (**Figure S43, S44**).  
539

540 **Discussion**

541

542 Our data reveal heterogeneity in coordinated gene expression and chromatin accessibility  
543 dynamics within individual cells during the critical early stages of a viral infection. By capturing  
544 the initial phases of EBV infection with high resolution -omics, we discern the gene regulatory  
545 environments associated with diverse infected cell fates and their respective developmental  
546 trajectories. These include genome-wide expression and chromatin signatures associated with  
547 effective host antiviral response, virus-triggered oncogene-induced senescence, and the path to  
548 sustained EBV latency and host cell immortalization, which is accessed via simulated B cell  
549 activation. Moreover, we develop a bioinformatic workflow to characterize post-infection  
550 outcomes through gene- and peak-level investigations at loci matching specific epigenetic  
551 patterns as well as host and viral transcription factor binding profiles. The combined high  
552 resolution multiomics data and integrative analytical framework reported herein yield a vividly  
553 detailed representation of the genome-wide interplay of host and virus.

554 We captured diverse post-infection B cell fate trajectories that, due to their asynchronous  
555 parallel emergence, cannot be resolved by ensemble sequencing methods. Remarkably, we find  
556 that large-scale euchromatin-to-heterochromatin transitions (20-40% reductions in genome-wide  
557 accessibility) can occur in post-infection trajectories and fates, including several that display  
558 increases in transcript levels. The scATAC data implicate Simpson's paradox with respect to  
559 heterogeneous chromatin accessibility dynamics following infection, since the total number of  
560 unique peaks increases in early infected populations while the peaks per cell can, in fact,  
561 decrease ([Simpson, 1951](#); [Trapnell, 2015](#)) (**Table S1**).

562 Global epigenetic silencing via SAHF formation ([Di Micco et al., 2011](#)) is most prominent both  
563 in cells that rapidly undergo innate sensing-mediated arrest and in cells that evade this response  
564 but arrest due to DNA damage response activation during virus-induced hyperproliferation. Our  
565 data also indicate a possible role for ribosome biogenesis in the transition from virus-induced  
566 arrest to senescence, likely through a p53-MDM2 axis ([Deisenroth and Zhang, 2010](#)), which  
567 critically regulates EBV transformation ([Forte and Luftig, 2009](#)). Intriguingly, the trajectory of  
568 successful infection is distinguished by increased accessibility at key sites against the larger  
569 backdrop of heterochromatin formation. A substantial number of these sites (many associated  
570 with viral TFs) have predicted *cis* linkages to genes enriched for regulation of apoptosis, tumor  
571 suppression, inflammation, and chromatin remodeling, all of which are determinants of successful  
572 EBV infection. Moreover, viral episome ATAC profile heterogeneity across infected phenotypes

573 indicates that latency establishment depends on retained accessibility to viral genes within the  
574 repressive host milieu.

575 The identification of an EBV-infected analog of an AP-eMBC phenotype is consistent with  
576 results from *in vitro* and *in vivo* antigen stimulation experiments ([Suan et al., 2017](#); [Taylor et al., 2015](#)), as well as previous work from our lab that identified CCR6 as an EBV Latency IIb program  
577 biomarker that becomes downregulated in the transition to Latency III in LCLs ([Messinger et al., 2019](#)). The development of this state *in vitro* implies that EBV may gain access to the memory  
578 pool *in vivo* via progenitors that have limited involvement in the GC reaction. In the context of  
579 normal antigen stimulation, this subset of eMBCs undergoes early exit from the cell cycle and GC  
580 reaction as a consequence of restricted access to or engagement with cognate antigen ([Glaros et al., 2021](#)). It is thus conceivable that EBV-infected B cells may differentially develop into GC  
581 BCs, PBs, or eMBCs from the AP state in a manner dependent on the extent to which the LMPs,  
582 EBNA and other viral gene products induce mimicry of BCR activation and signaling. This model  
583 accommodates a surprising possibility – that EBV may access long-term persistence and survival  
584 not only within post-GC high-affinity MBCs but also via GC-independent eMBCs that avoid  
585 extensive proliferation.

586 The activated B cell and plasmablast phenotypes that developed within 5 days are generally  
587 consistent with our findings in LCLs ([SoRelle et al., 2021](#)) and resemble *in vivo* tonsil cell subset  
588 transcriptomes. Furthermore, differentiated plasmablasts exhibited fewer accessible sites in both  
589 host chromatin and viral episomes relative to activated cells. Notably, prior studies found that only  
590 50% of EBV-infected cells that secrete immunoglobulin go on to become immortalized ([Tosato et al., 1985](#)). Additional work within LCLs demonstrated that EBV<sup>+</sup> cells with upregulated Ig  
591 production exhibited reduced DNA synthesis and EBNA downregulation ([Wendel-Hansen et al., 1987](#)). Collectively, these findings support a model for continuous EBV-driven B cell differentiation  
592 *in vitro*, wherein plasmablasts are continually generated through activation-induced maturation  
593 yet selected against by their reduced proliferation. While this disadvantage limits viral replication  
594 via cell division, the reduced MYC levels, increased XBP1, and endoplasmic reticulum stress in  
595 these cells may support EBV lytic reactivation ([Guo et al., 2020](#); [Laichalk and Thorley-Lawson, 2005](#); [Sun and Thorley-Lawson, 2007](#); [Taylor et al., 2011](#)).

600 Depending on the phenotype comparison, roughly 10-35% of all DEGs were correlated with  
601 DAPs. This range was similar to the frequencies of both differential accessibility of expressed TF  
602 binding motifs (23%) and DEGs associated with differentially accessible promoters (25%)  
603 identified in dexamethasone-treated A549 cells profiled with sci-CAR ([Cao et al., 2018](#)). The  
604 observation of similar DAP-linked DEG frequencies in response to diverse stimuli (e.g., chemically

607 induced glucocorticoid receptor activation, viral infection) raises intriguing questions regarding the  
608 fundamental frequency of genes regulated, at least in part, by accessibility changes. The  
609 observed proportion implies that most DEGs may be regulated by higher order chromatin  
610 interactions and differential recruitment of transcriptional activators and/or RNA Pol II.

611 The crisp-ATAC method provides a simple, flexible informatic approach to map ChIP-seq  
612 profiles to cell phenotypes discovered from scATAC-seq. Thus, it provides a potential route for  
613 effectively bootstrapping scATAC resolution to datasets from other -omics modalities. When data  
614 from suitable reference cell types and/or states are available, crisp-ATAC can be used to predict  
615 phenotype-resolved gene regulation by evaluating simple or complex combinations of factor  
616 binding sites, histone modifications, and/or nuclear chromatin compartmentalization across all  
617 differentially accessible sites. In our case, cell-matched empirical scRNA-seq data can be cross-  
618 referenced with crisp-ATAC outputs for methodological validation and identification of genes of  
619 interest for future studies. This method is adaptable to comparisons of phenotype-resolved ATAC  
620 profiles in contexts such as other infections, development, and cell responses to stimuli or  
621 therapies. We expect this approach to be particularly powerful for exploring TF-associated  
622 regulatory changes in time-resolved studies of cellular behaviors.

623 The identification and characterization of genome-wide EBV infection dynamics within *FCRL4*<sup>+</sup>  
624 TLM B cells (as well as other B subsets including *FCRL4*<sup>+</sup> / *TBX21*<sup>-</sup> and *FCRL4*<sup>-</sup> / *TBX21*<sup>+</sup> B cells  
625 evident within our data) provides an intriguing road map for subsequent research into EBV  
626 pathogenesis in unique B cell niches and their potential role(s) in human disease. Specifically,  
627 the tissue-homing capacity, innate immune mediation roles, and progenitor-like features of TLM  
628 B cells make them a high-interest target cell type in a range of cancers and autoimmune  
629 conditions. Notably, *TBX21* and *CXCR3* have separately been found at high frequencies in  
630 specific B cell lymphoma subtypes including Chronic Lymphocytic Leukemia (CLL), splenic  
631 marginal zone lymphoma (SMZL), extranodal marginal zone lymphoma (EMZL), precursor B-cell  
632 Lymphoblastic Leukemia, and Hairy Cell Leukemia ([Dorfman et al., 2004](#); [Jones et al., 2000](#)).  
633 Generally, it has been observed that expansion of B cells with a base expression profile of low  
634 CD21 (CR2) and inhibitory receptors including *FCRL4* is a fundamental feature of chronic  
635 infections and (auto) immune disorders ([Freudenhammer et al., 2020](#)). Expanded atypical MBC  
636 populations expressing *FCRL4* and *ITGAX* have been identified in patients with chronic  
637 *Plasmodium falciparum* infections living in regions with endemic malaria ([Weiss et al., 2009](#)) and  
638 in exhausted B cell populations (also *CXCR3*<sup>+</sup>) described in the context of HIV viremia ([Moir et  
639 al., 2008](#)). *FCRL4*<sup>+</sup> / *TBX21*<sup>+</sup> / *ITGAX*<sup>+</sup> B cells have also recently been identified as a pathogenic  
640 subset in primary Sjögren's Syndrome (pSS) with lymphomagenic potential ([Verstappen et al.,](#)

641 [2020](#)). FCRL4<sup>+</sup> / CD20<sup>hi</sup> B cells expressing RANKL/TNFSF11 have been reported as a subset  
642 that contributes to inflammation in rheumatoid arthritis (RA) ([Yeo et al., 2015](#)) – this matches an  
643 additional phenotype that we observed in ALRA-imputed data from Day 8 and in the GM12878  
644 LCL. Notably, RANKL/TNFSF11 was not expressed in these cells until after EBV infection (data  
645 not shown). A variety of B cells phenotypes have been found to be clonally expanded in systemic  
646 lupus erythematosus (SLE). These include CXCR3<sup>+</sup>/CD19<sup>hi</sup> B cells ([Nicholas et al., 2008](#)),  
647 FCRL4<sup>-</sup> DN2 cells ([Jenks et al., 2018](#)) and notably, a recent large cohort study identified IL-21  
648 stimulation drove expansion of tissue-homing CD11c<sup>+</sup> / T-bet<sup>+</sup> (*ITGAX*<sup>+</sup> / *TBX21*<sup>+</sup>) with significantly  
649 elevated levels of FCRL3, FCRL4, and FCLR5 ([Wang et al., 2018](#)). In the context of autoimmunity,  
650 comprehensive analysis of distinct B cell subsets – including how each of these may be affected  
651 by EBV infection – is especially relevant to resolving the etiology of multiple sclerosis (MS). While  
652 one report found clonally expanded B cells from the cerebrospinal fluid (CSF) of MS patients with  
653 upregulated TBX21, CXCR3, and SOX5, EBV reads were not identified in the samples ([Ramesh  
654 et al., 2020](#)). However, two recent reports that provide epidemiological ([Bjornevik et al., 2022](#))  
655 and serological ([Lanz et al., 2022](#)) data supporting a causal role for EBV in at least some MS  
656 cases have ignited efforts to explore the mechanistic foundations of this causality. That effort,  
657 along with research into other diseases associated with EBV-induced B cell dysregulation, will  
658 benefit from understanding the nuances of viral pathogenesis in distinct B cell niches. The data  
659 developed and analyzed herein provide a comprehensive portrait of *de novo* EBV infection within  
660 the canonical GC model and offer a tantalizing initial glimpse into non-canonical infection  
661 dynamics in at least one atypical yet critical B cell phenotype. These non-canonical responses to  
662 EBV infection are exemplified by the apparent lineage-inappropriate expression of genes that  
663 mediate neural cell development, adhesion, and signaling within a lymphoid compartment. By  
664 combining high resolution, scale, and modalities, we hope this resource will facilitate advances in  
665 our understanding of the gene regulatory diversity intrinsic to peripheral B cell subsets and how  
666 that heterogeneity underlies previously obscured complexities of host-EBV dynamics.  
667

#### 668 Limitations of the study

669 The reported single-cell multiomics data have several limitations. They do not capture aspects  
670 of host-virus dynamics acting at other molecular levels. Examples include epigenetic  
671 modifications (e.g., DNA methylation status), three-dimensional chromatin architecture changes,  
672 modulation of translation and protein abundance, post-translational modifications, protein-protein  
673 interactions, and signaling cascades (e.g., phosphorylation status). While we present a method

674 for inferring DAP-linked TF binding and epigenetic modifications based on empirical scATAC data,  
675 we do not have direct ChIP-seq measurements at the single-cell level.

676 The reported bioinformatic methodology (crisp-ATAC) also has notable constraints. This  
677 approach is limited by the availability of ChIP-seq data from an appropriate cell type and target  
678 reference state. Moreover, regulatory site predictions must be empirically tested to validate  
679 potential functions in gene expression control. Finally, distance limits imposed for identifying *cis*-  
680 regulatory linkages preclude identification of distal gene regulatory elements formed via 3D  
681 nuclear conformation.

682

683 **Acknowledgments**

684

685 The authors wish to thank members of the Duke University Molecular Genomics Core (MGC)  
686 and the Duke Center for Genomic and Computational Biology (GCB), especially Emily Hocke,  
687 Karen Abramson, Dr. Simon Gregory, and Dr. Nicolas Devos. Special thanks are also due to the  
688 anonymous donors, without whose blood donations this work would not have been possible.  
689 E.D.S. wishes to acknowledge funding support from the Department of Molecular Genetics and  
690 Microbiology Viral Oncology Training Grant (NIH T32 # 5T32CA009111-42). This work was  
691 supported by funding from the National Institute of Dental and Craniofacial Research (NIDCR  
692 award #R01DE025994-06).

693 **Experimental Methods**

694

695 PBMC isolation and B lymphocyte enrichment

696 Whole blood (50 mL each from two anonymous donors; TX1241/Donor 1 & TX1242/Donor 2)  
697 was obtained from the Gulf Coast Regional Blood Center (Houston, TX). Upon receipt, peripheral  
698 blood mononuclear cells (PBMCs) from each donor sample were isolated via Ficoll gradient  
699 separation (Histopaque®-1077, Sigma #H8889), resuspended at  $10 \times 10^6$  cells/mL in RPMI 1640  
700 + 15% heat-inactivated fetal bovine serum (FBS, v/v, Corning) (R15 media), and incubated  
701 overnight at 37°C and 5% CO<sub>2</sub>. The next day, CD19<sup>+</sup> B cells were enriched from donor PBMCs  
702 via negative isolation (BD iMag Negative Isolation Kit, BD Biosciences #558007) and  
703 resuspended at  $2 \times 10^6$  cells/mL in R15 supplemented with 2 mM L-glutamine, 100 units/mL  
704 penicillin, 100 µg/mL streptomycin, and 0.5 µg/mL cyclosporine A (R15<sup>+</sup> media). Roughly  $45 \times 10^6$   
705 B cells were recovered per donor post-enrichment. Following CD19<sup>+</sup> validation (see below: Flow  
706 cytometry), enriched B cell aliquots (1-2 mL at  $3 \times 10^6$  cells/mL) were viably frozen in 90% FBS +  
707 10% DMSO and stored in liquid N<sub>2</sub>.

708

709 EBV infection and cell culture

710 The type 1 EBV strain B95-8 was obtained in-house as viral supernatant from the inducible  
711 B95-9 Z-HT cell line as reported previously ([Johannsen et al., 2004](#)). Immediately after  
712 withholding and cryopreserving uninfected enriched B cells for each donor (day 0 samples), the  
713 remaining cells in culture were infected with B95-8 via resuspension in viral supernatant (100 µL  
714 per  $1 \times 10^6$  cells) for 1 h at 37°C and 5% CO<sub>2</sub>. Infected B cells from each donor were rinsed with  
715 1x PBS, resuspended in R15<sup>+</sup> media, and incubated at the conditions described above throughout  
716 the course of infection. Aliquots were taken from each infected donor culture at 2-, 5-, and 8-days  
717 post-infection and viably frozen as described for uninfected day 0 samples.

718

719 Flow cytometry

720 The extent of B cell enrichment was quantified for each donor using flow cytometry. Following  
721 negative isolation, cell samples ( $2 \times 10^5$  per donor) were rinsed with FACS buffer (1x PBS + 2%  
722 FBS), stained with phycoerythrin (PE)-conjugated mouse anti-human CD19 (BioLegend, clone  
723 HIB19; catalog #302208; lot #B273508) in the dark for 30 min at room temperature, then rinsed  
724 again prior to analysis. Cell samples at each timepoint were prepared as described and co-stained  
725 with PE-anti-CD19 and allophycocyanin-conjugated mouse anti-human CD23 (APC-anti-CD23,  
726 BioLegend, clone EBVCS-5; catalog #338513; lot #B273489) to validate successful EBV

727 infection. To validate the AP-eMBC phenotype (c0), enriched resting B cells from two additional  
728 donors (TX1253 and TX1254) were labeled with CellTrace Violet (ThermoFisher / Invitrogen, Cat  
729 #34571) and stained with one of the following combinations at days 0, 2, 5, and 8: CCR6/Memory  
730 panel (FITC-anti-CD27, PE-anti-CCR6, and APC-anti-CD23); Naïve/Memory panel (FITC-anti-  
731 IgD, PE-anti-CD19, and APC-anti-CD27); or CCR6/Naïve panel (FITC-anti-IgD, PE-anti-CCR6,  
732 and APC-anti-CD23). FITC-anti-CD27, FITC-anti-IgD, and APC-anti-CD27 were purchased from  
733 BioLegend (Cat #302806, #348206, and #356410, respectively) and PE-anti-CCR6 was  
734 purchased from Invitrogen (Cat #12-1969-42). Compensation matrices were calculated from  
735 single-stain controls for FITC and PE and applied to all samples for analysis. All cytometry  
736 measurements were acquired with a BD FACSCanto II (BD Biosciences) and analyzed using  
737 FlowJo version 10 (Ashland / BD Biosciences).

738

739 Human tonsil sample preparation

740 Tonsillar B cells were isolated from discarded, anonymized tonsillectomies from the Duke  
741 Biospecimen Repository and Processing Core (BRPC; Durham, NC). Tonsil tissue samples were  
742 manually disaggregated, filtered through a cell strainer, and isolated by layering over a cushion  
743 made from Histopaque-1077 (H8889; Sigma-Aldrich). Harvested lymphocytes were washed three  
744 times with FACS buffer (5% FBS in PBS) prior to scRNA library preparation.

745

746 Preparation of scRNA and scATAC libraries

747 Cryopreserved samples from each early infection timepoint of interest were simultaneously  
748 thawed by donor and purified to > 90% viable cells by Ficoll gradient separation. Viable cells from  
749 each timepoint and donor were then prepared as single-cell matched gene expression (scRNA)  
750 and chromatin accessibility (scATAC) libraries by the Duke Molecular Genomics Core staff with  
751 the 10x Chromium Next GEM Single Cell Multiome ATAC + Gene Expression Kit (10x Genomics,  
752 Pleasanton, CA) ([Satpathy et al., 2019](#); [Zheng et al., 2017](#)). Briefly, nuclei were isolated from  
753 each sample and subjected to transposition at accessible chromatin sites. Next, transposed  
754 nuclei, barcoding master mix, and gel beads containing unique barcode sequences were  
755 prepared into single-cell GEMs (Gel bead emulsions) using the Chromium Controller and Chip J.  
756 Within each GEM, poly-adenylated (poly-A) mRNA transcripts from individual nuclei are captured  
757 by barcoded, indexed poly-T primers and reverse transcribed into cDNA. Simultaneously, a  
758 separate barcoded sequence containing a spacer and Illumina P5 adaptor sequence is added to  
759 transposed regions within the captured nucleus. Barcoded multiomes were then purified, pooled,  
760 and pre-amplified by PCR prior to library construction. The scATAC library for each sample is

761 generated by PCR amplification and incorporation of sample index and Illumina P7 adaptor  
762 sequences. Separately, pre-amplified gene expression cDNA is further PCR amplified,  
763 fragmented, and size selected. The scRNA library for each sample is then constructed using PCR  
764 to incorporate the P5 and P7 sequencing adaptors. Two biological replicates of tonsillar  
765 lymphocytes were prepared as scRNA libraries using the 10x Genomics Next GEM 3' Gene  
766 Expression kit with v3 chemistry (10x Genomics, Pleasanton, CA), and sequenced, processed,  
767 aligned, and analyzed as described above for early infection scRNA samples.

768

769 Sequencing, alignment, and count matrix generation

770 The 8 paired-end scATAC libraries (4 timepoints per 2 donors) were pooled onto two lanes of  
771 an Illumina S2 flow cell and sequenced at a target depth of 25,000 reads per cell on an Illumina  
772 NovaSeq (Illumina, San Diego, CA). The 8 paired-end scRNA libraries were similarly pooled and  
773 sequenced at a target depth of 50,000 reads per cell. Tonsil scRNA libraries were likewise pooled  
774 and sequenced at 50,000 reads per cell. All sequencing runs were performed by staff at the Duke  
775 Center for Genomic and Computational Biology. Raw base calls for each assay were prepared  
776 as sample-demultiplexed FASTQ files using *cellranger-arc mkfastq* (Cellranger, 10x Genomics),  
777 a wrapper of the Illumina *bcl2fastq* function. Next, sample-matched scRNA and scATAC reads  
778 were aligned against genomic references to produce multiome count matrices using *cellranger-arc  
779 count*. One set of count matrices was generated by mapping reads to a concatenated genomic  
780 reference constructed from the human genome (GRCh38) with the ~172 kB type 1 EBV genome  
781 (NC\_007605) included as an extra chromosome. These outputs were used for downstream RNA-  
782 only analyses to capture host and viral gene expression. A second set of count matrices  
783 generated by mapping to GRCh38 only was used for downstream joint RNA and ATAC analyses.  
784 Compatible reference packages were assembled from the relevant genome (.fa) and annotation  
785 (.gtf) files using *cellranger-arc mkref*.

786

787 Data QC and scMultiome analysis

788 All direct analysis of scRNA and scATAC data was conducted in R using Signac ([Stuart et al.,  
789 2021](#)), an extension of Seurat ([Macosko et al., 2015](#); [Satija et al., 2015](#); [Stuart et al., 2019](#)).  
790 Following read mapping and counting, linked scRNA and scATAC data were obtained from  
791 between 8,934-20,000 cells per sample. After QC filtering by mitochondrial expression (n < 20%),  
792 total transcripts (n < 25,000), unique transcripts (n > 1,000), and minimum cells expressing a  
793 given feature (n > 3), data from between 8,376-19,310 cells per sample were analyzed (see **Table  
794 S1**). The mitochondrial gene expression threshold was selected based on the high metabolic

795 activity of early-infected B cells and the high cell viability observed in each sample (> 90%)  
796 immediately prior to library preparation to preserve biologically relevant phenotypes ([Osorio and](#)  
797 [Cai, 2021](#)). After QC filtering, a total of 52,271 and 44,920 cells were analyzed across the infection  
798 timecourse for donors TX1241 and TX1242, respectively. For RNA-only analysis, gene  
799 expression data (host and viral) across all timepoints for a given donor were merged into a single  
800 object, log normalized, scored for cell cycle markers, and scaled with cell cycle scoring regressed  
801 out. The top 2,000 differentially expressed features over the early infection timecourse data were  
802 identified and used for principal component analysis (PCA). The top 30 principal components  
803 were further dimensionally reduced via uniform manifold approximation projection (UMAP,  
804 ([McInnes et al., 2018](#))), and clustering was performed to identify biologically distinct cell  
805 subpopulations. Merged scRNA dataset pseudotime trajectories were calculated using Monocle3  
806 ([Qiu et al., 2017](#)), and were mapped along with cluster identities to 3D UMAP coordinates for  
807 visualization ([Qadir, 2019](#); [Qadir et al., 2020](#)). For joint ATAC and RNA analysis, host gene  
808 expression and chromatin accessibility were analyzed for each separate timepoint and for a  
809 merged object containing Day 0 and Day 8 multiome data. Nucleosome signal and transcription  
810 start site (TSS) enrichment were calculated and used for QC filtering (Nucleosome.signal < 2,  
811 TSS.enrichment > 1). ATAC peaks were called using macs2 ([Liu, 2014](#)) with hg38 annotations.  
812 Gene expression data in the joint analysis was processed as described for the RNA-only analysis  
813 with the exception of using Signac's SCTransform function instead of log normalization for  
814 expression counts. Top differential features in each assay ('peaks' and 'SCT') were determined,  
815 and multimodal neighboring and UMAP were performed for integrated data visualization. Cluster  
816 identities defined in the RNA-only assay were mapped to this merged joint dataset, which  
817 contained cells representing all identified subpopulations. Peaks with significant (anti-) correlation  
818 ( $p < 0.05$  for z-score of correlation coefficients) to differentially expressed genes were identified  
819 using the LinkPeaks function in Signac, which was informed by SHARE-seq ([Ma et al., 2020](#)).  
820

#### 821 crispATAC workflow and reference data curation

822 ChIP-referenced inference from single-cell phenotype ATAC (crispATAC) was developed to  
823 predict subpopulation-resolved gene regulatory features. In a typical workflow, cluster-level  
824 chromatin accessibility tracks are cross-referenced against ChIP-Seq (Chromatin  
825 Immunoprecipitation Sequencing) profiles for epigenetic marks and TFs of interest measured from  
826 a reference cell phenotype (in this study, lymphoblastoid cell lines such as GM12878). In this  
827 study, cluster-specific called peaks from the joint scATAC + scRNA dataset were extracted and  
828 prepared as simplified genomic range files (3-column .bed file format). Next, the desired ChIP-

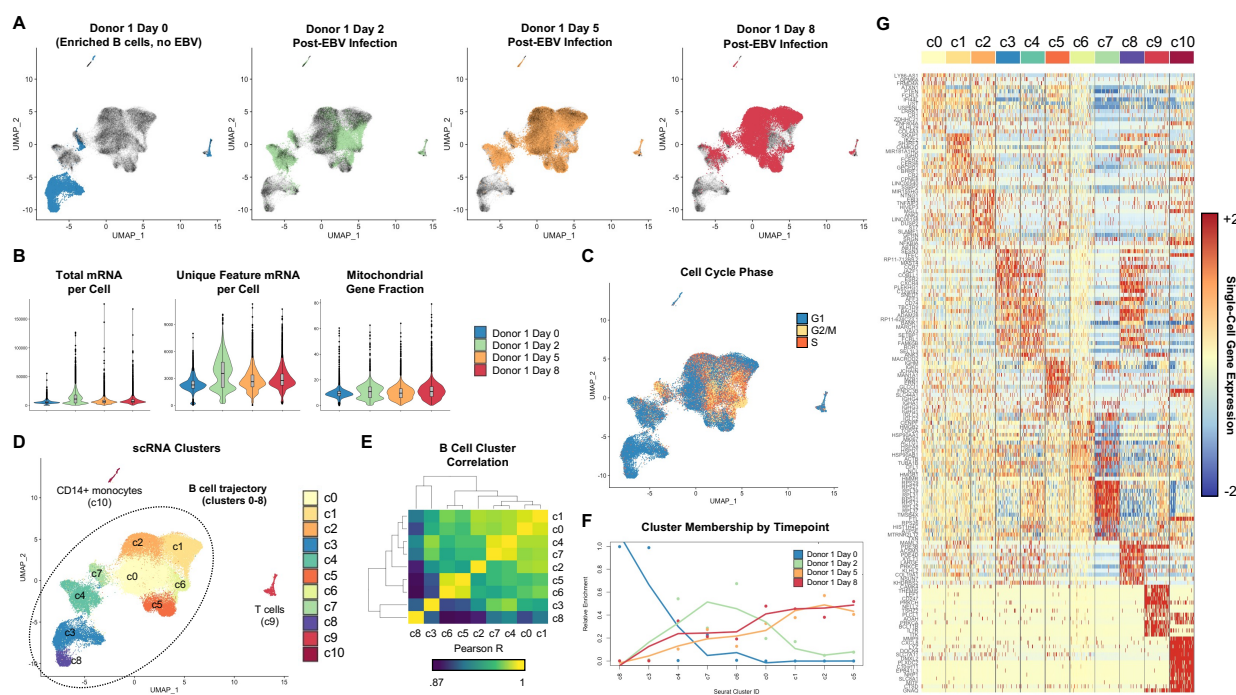
829 Seq datasets for the reference phenotype were downloaded and, where applicable, converted to  
830 .bedgraph format to be used as input for peak calling with the *macs2* function *bdgpeakcall*. The  
831 ChIP (and Hi-C) datasets used for crispATAC in this study (**Table S2**) are all publicly available  
832 from the National Center for Biotechnology Information (NCBI) Gene Expression Omnibus (GEO).  
833 Once all ATAC-seq and ChIP-seq peak files were generated, all were used as inputs to a single  
834 call of the bedtools ([Quinlan and Hall, 2010](#)) function *multiinter*, which output a matrix of all  
835 genomic range intersection intervals where at least one input file exhibited a peak. This  
836 intersection matrix was imported to R as a data frame and analyzed to identify common and/or  
837 differential intervals (matrix rows) among scATAC cluster phenotypes, epigenetic marks, and TFs  
838 using Boolean logic gating by dataset (matrix columns). For a given crispATAC recipe (e.g., peaks  
839 in scATAC cluster 1 not in scATAC cluster 2 intersected with EBNA2 ChIP peaks =  $[c1 \cap !c2] \cap$   
840 EBNA2), the genome intervals matching the gating criteria were returned and converted to .bed  
841 files. Lists of differentially accessible, transcription-factor associated sites generated in this way  
842 were subsequently analyzed with the Genomic Regions Enrichment of Annotations Tool (GREAT)  
843 ([McLean et al., 2010](#)) to identify potential *cis*-regulated genes within 1 megabase of each query  
844 site. As a final step, output lists of potential linked genes were intersected with the top marker  
845 genes identified from the corresponding cluster-wise comparison in the scRNA assay, thus  
846 integrating direct single-cell RNA and ATAC measurements with subpopulation-resolved  
847 regulatory inferences from ensemble ChIP profiles. In a similar but separate approach, scATAC  
848 and ChIP peaks were intersected with topologically associated domain (TAD) boundaries  
849 (prepared using hicExplorer, ([Ramírez et al., 2018; Wolff et al., 2018; Wolff et al., 2020](#))) and  
850 nuclear subcompartments from GM12878 Hi-C data to study differentially accessible TF-  
851 associated sites in the context of 3D nuclear architecture.

852

#### 853 Visualization of crispATAC outputs, gene ontologies, and networks

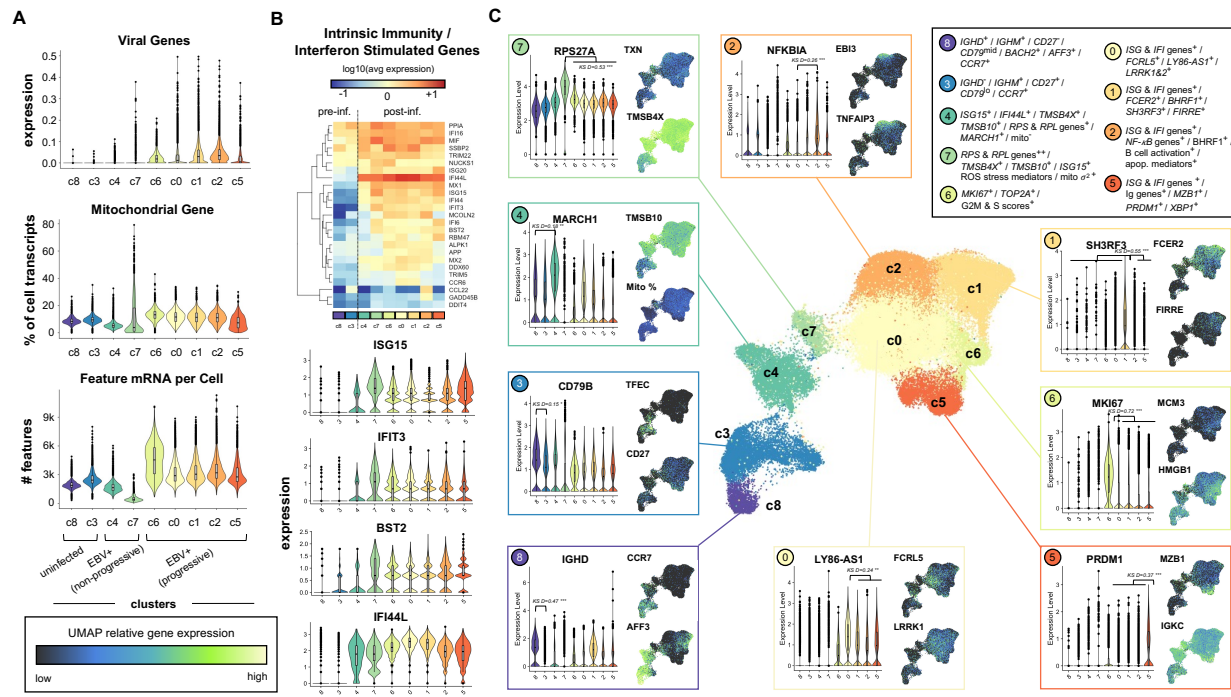
854 Data for genes of interest identified from crispATAC recipes were explored using dimensionally  
855 reduced (UMAP) expression maps and cluster-level accessibility tracks (Signac, ([Stuart et al.,](#)  
856 [2021](#))), called peaks aligned with TFs and epigenetic marks (IGV, ([Robinson et al., 2011](#))), and  
857 local neighborhoods in Hi-C contact maps (Juicebox, ([Durand et al., 2016](#))). Cluster-resolved  
858 gene ontologies were generated and quantified by GREAT ([McLean et al., 2010](#)). Top scRNA  
859 assay cluster markers and GREAT output gene lists were also visualized as annotated networks  
860 using Cytoscape ([Shannon et al., 2003](#)).

861 **Main Figures**  
862  
863



864  
865  
866 **Figure 1. Time-resolved single-cell gene expression during early EBV infection of B**  
867 **lymphocytes**

868 (A) Single-cell gene expression timecourse data from early EBV infection.  
869 (B) General expression trends during early infection. Total mRNA refers to all transcripts captured,  
870 while Feature mRNA refers to the number of unique transcripts (per cell).  
871 (C) Cell phase scoring of expression data after cell cycle marker regression.  
872 (D) Unsupervised clustering of early infected cell expression in merged timepoint data.  
873 (E) Pairwise correlation of identified clusters.  
874 (F) Cluster membership by timepoint. Fit lines show coarse changes in phenotype frequency over  
875 time.  
876 (G) Single-cell expression of the top 15 gene markers by cluster.  
877 See also *Figures S1-S4*



879  
880

## 881 Figure 2. High-resolution dissection of infected B cell phenotypes

882 (A) Overview of global gene expression trends by phenotype.  
 883 (B) Induction of interferon response genes in all EBV<sup>+</sup> clusters.  
 884 (C) Phenotype-resolved transcriptomic signatures in resting and EBV<sup>+</sup> B cells. Select cluster-  
 885 resolved comparisons of gene expression were evaluated via the Kolmogorov-Smirnov D statistic  
 886 (KS D) and associated p value (\* p < 1e-5; \*\* p < 1e-10; \*\*\* p < 1e-15) from 500 randomly sampled  
 887 cells per cluster.  
 888 See also Figures S5-S11  
 889

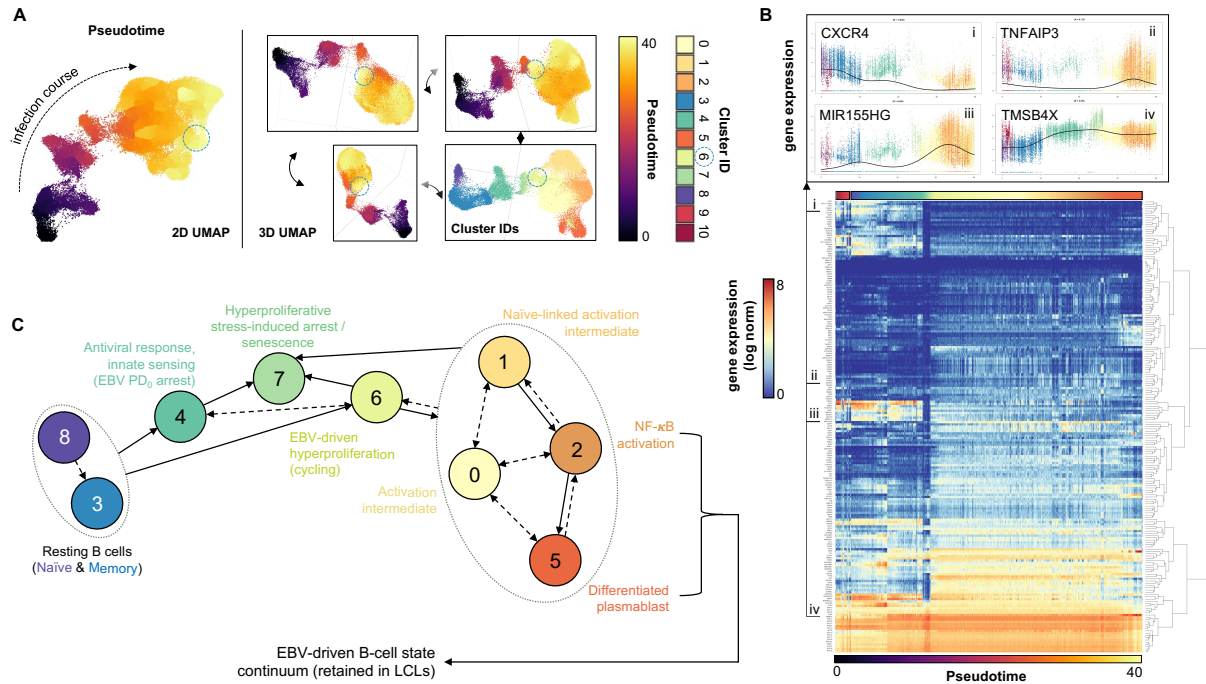


### Figure 3. A model of B cell fate trajectories in early EBV infection

(A) Monocle3 pseudotime scoring of merged timecourse expression data relative to resting B cells (day 0). Unlike the 2D UMAP, 3D UMAPs depict closer proximity of c6 (first observed at day 2, blue dashed circle) to resting cells, consistent with the temporal emergence of the c6 phenotype prior to the c0, c1, c2, and c5 phenotypes.

(B) Pseudotime-resolved expression dynamics of top differentially expressed genes (DEGs) across phenotypes. Genes are hierarchically clustered by pseudo-temporal expression pattern similarity. Spline interpolant fits are shown for expression of select genes in pseudotime (insets i-iv). After sorting cells by pseudotime score in ascending order, the average pseudotime score of every 25-cell interval was computed for efficient visualization (i.e., pseudotime for 52,271 cells at 25 cell resolution).

(C) Annotated state model of EBV<sup>+</sup> B cell phenotypes and fate trajectories. Empirically observed and putative directed state transitions are depicted in solid and dashed edges, respectively. Edges drawn to groups of phenotypes (dotted ovals) indicate transitions to/from each cluster within the group.

See also Figures S12-S19

890  
891

892

893

894

895

896

897

898

899

900

901

902

903

904

905

906

907

908

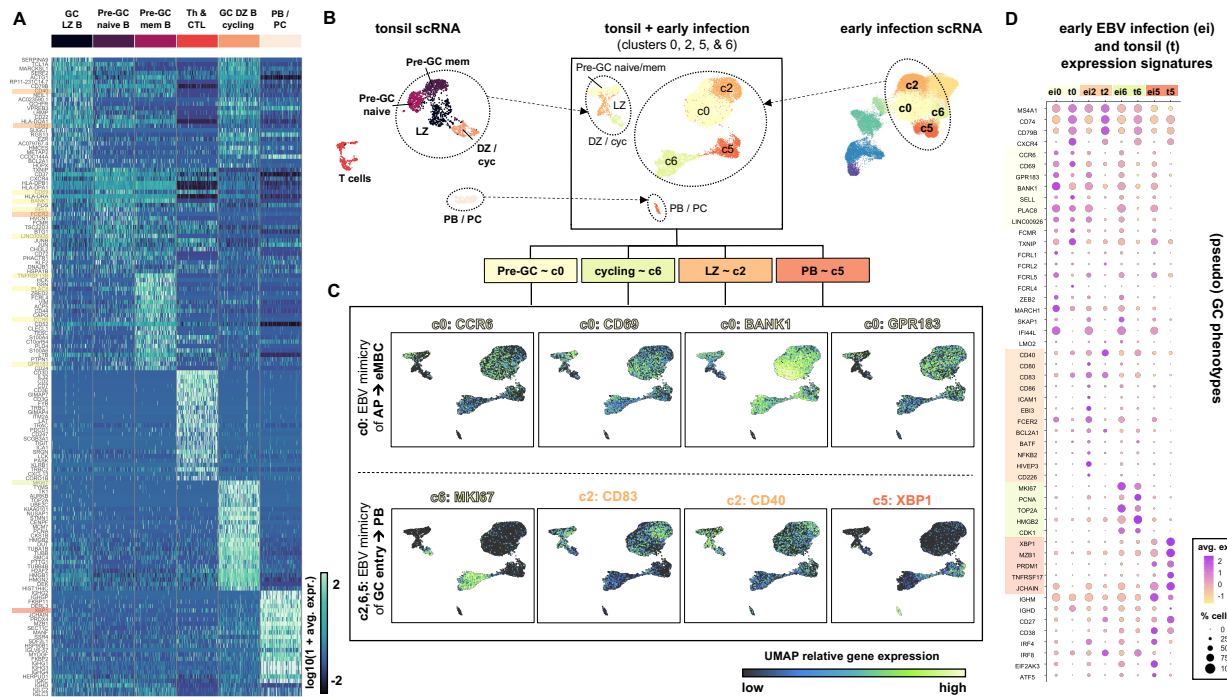


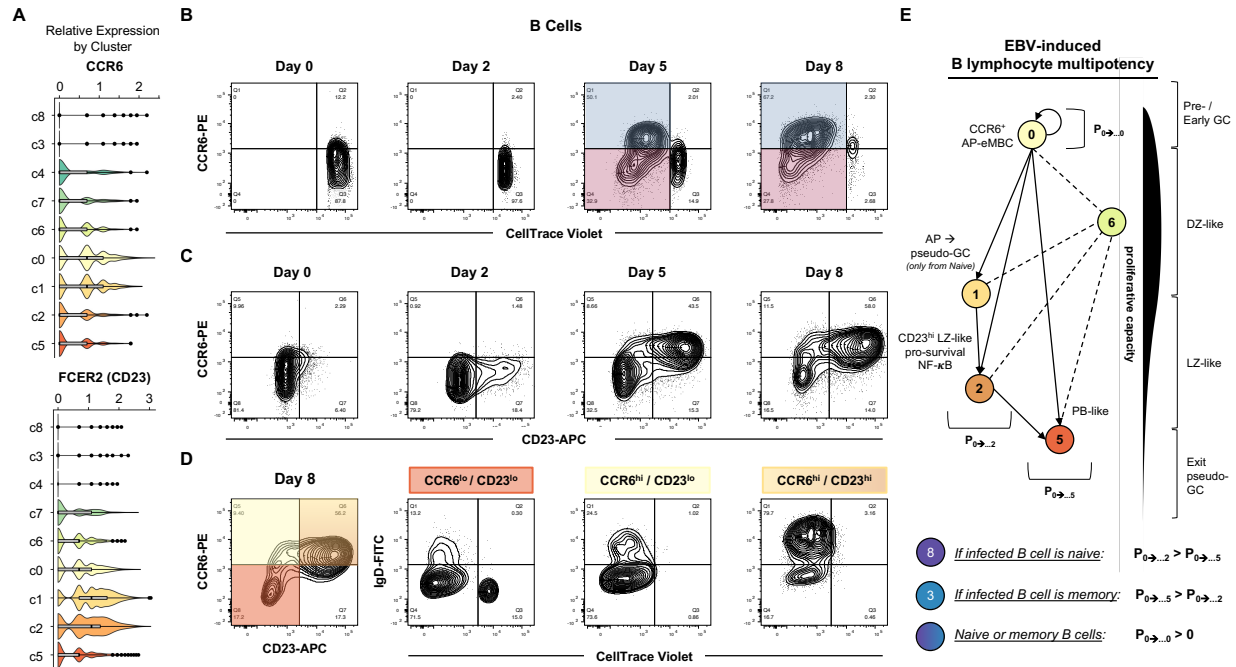
**Figure 4. A subset of early infected cells exhibits hallmarks of a multipotent activated precursor to early memory B cells (eMBCs)**

(A) Top phenotype markers of healthy human tonsil subsets identified from scRNA-seq.

(B) UMAP merging of tonsil and key early infection cluster scRNA-seq assays. Tonsil clusters are colored to match the closest corresponding cells from early infection.

(C) UMAP Correspondence of key gene expression across tonsillar subsets and early infection phenotypes. Select markers of multipotent progenitors and eMBCs were informed by data from [\(Suan et al., 2017\)](#) and [\(Glaros et al., 2021\)](#).

(D) Dot plot visualization of key genes across early infection (ei) c0, c2, c5, and c6 and their analogs within tonsils (t).



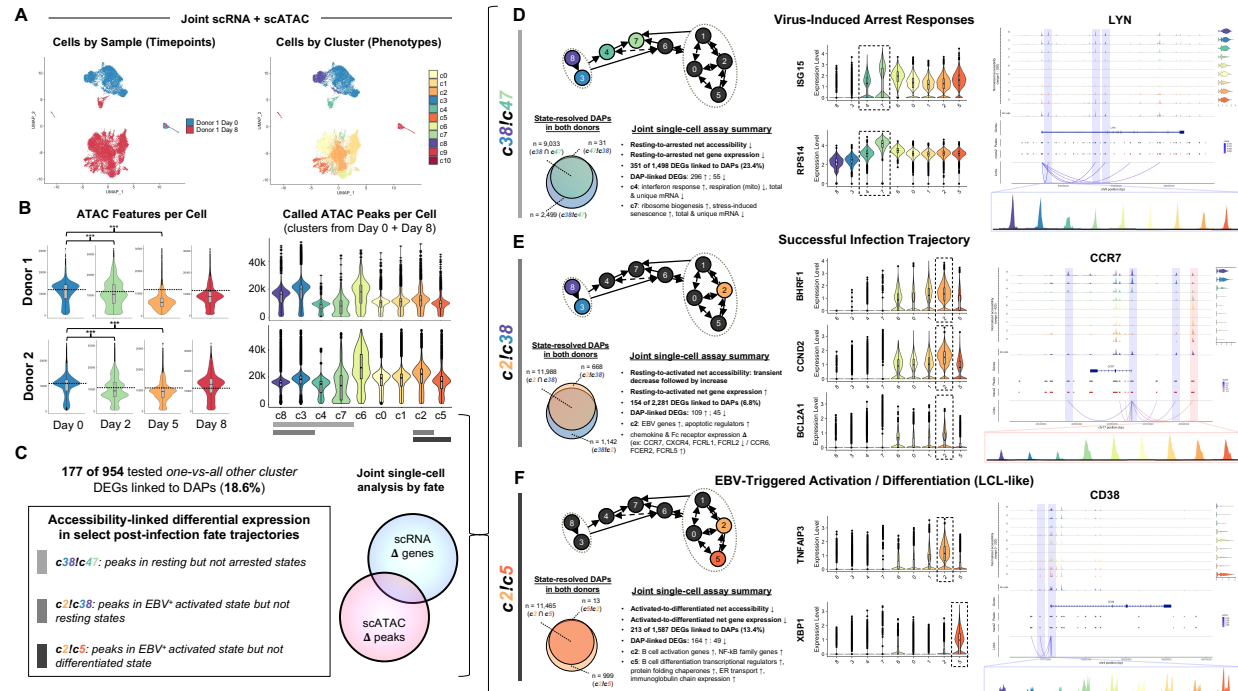


**Figure 6. Cell-matched expression and chromatin accessibility cell fate trajectories**

(A) UMAP visualization of scRNA + scATAC data generated using weighted nearest neighbors (WNN) multimodal integration (Hao et al., 2021; Stuart et al., 2020). Merged multimodal data from the first and last timepoints (day 0 & day 8) contain cells representative of all identified phenotypes.

(B) Distribution of called ATAC peaks per cell by timepoint and phenotype in both donors (\*\*p < 1e-15, one-sided Kolmogorov-Smirnov test).

(C) Overview of global differentially accessible peak (DAP) -linked differentially expressed genes (DEGs) and cluster comparisons for major trajectories of interest. DAPs are identified by their presence in one or more peaks but not in (!) one or more other peaks. DAP-linked DEGs were explored in resting versus arrested cells (c38 vs c47), EBV<sup>+</sup> activated versus resting cells (c2 vs c38), and EBV<sup>+</sup> activated vs EBV<sup>+</sup> differentiated cells (c2 vs c5).

(D) Virus-induced arrest responses. State-resolved DAPs (c38/c47) and joint assay trend summaries are presented in addition to example DEGs and DAP linkages resolved by phenotype.

(E) Successful infection trajectory. State-resolved DAPs (c2/c38), joint assay summaries, and trajectory-specific examples are presented as in (D).

(F) EBV-induced B cell activation/differentiation continuum. State-resolved DAPs (c2/c5), joint assay summaries, and trajectory-specific examples are presented as in (D and E).

See also Figures S26-S38

939  
940

941  
942  
943  
944  
945  
946  
947  
948  
949  
950  
951  
952  
953  
954  
955  
956  
957  
958  
959  
960

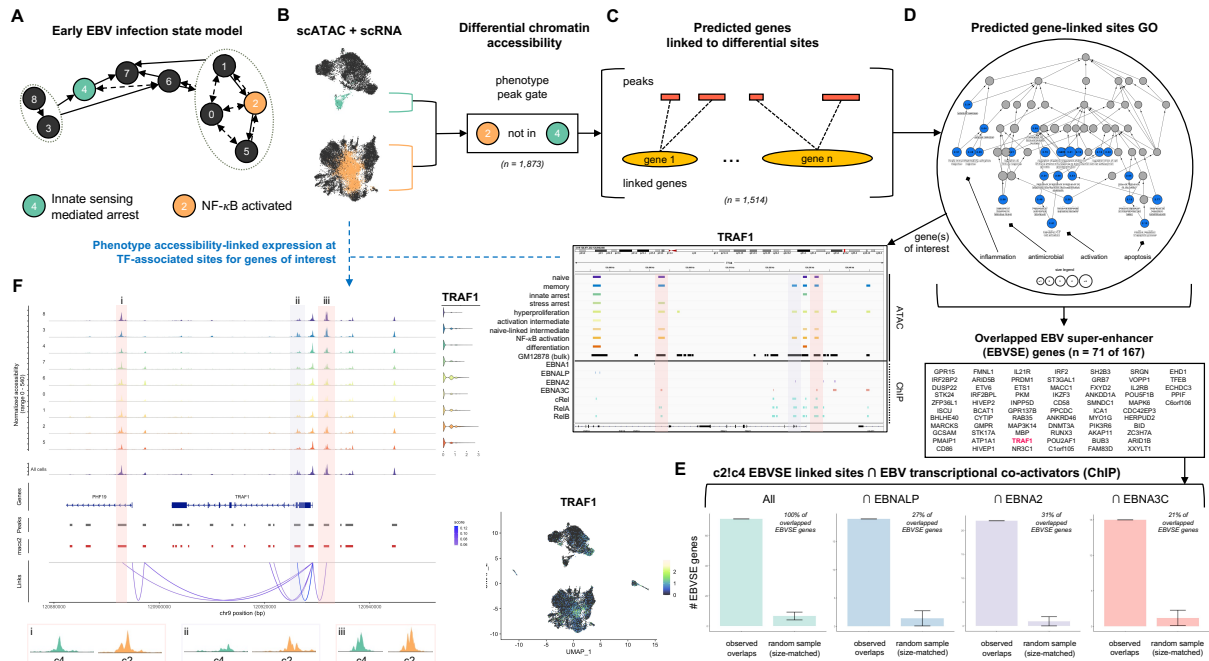


**Figure 7. crisp-ATAC analysis of DAP-linked DEGs in activated versus innate arrested EBV<sup>+</sup> B cells**

(A) Schematic of NF-κB activation (c2) and innate arrest (c4) model phenotypes.

(B) Multimodal assay gating to extract c2/c4 DAPs.

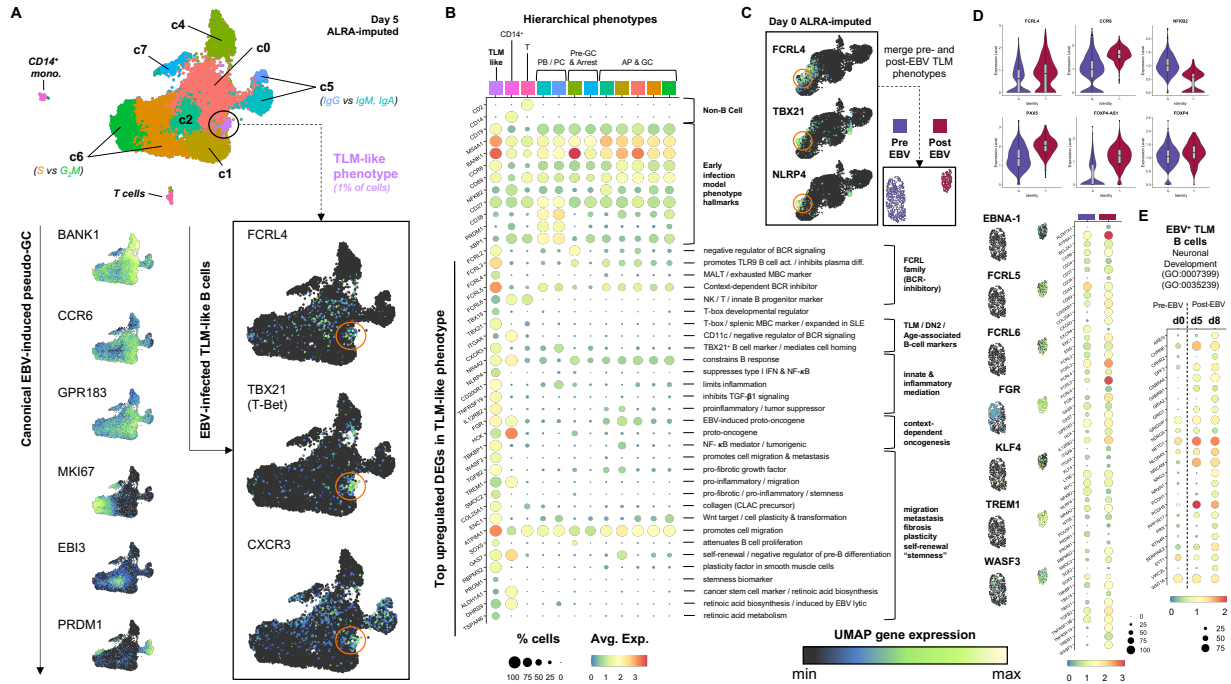
(C and D) Prediction of *cis*-regulatory linkage. All c2/c4 peak intervals (n=1,873) are used as inputs to the GREAT (McLean et al., 2010) to predict c2/c4 DAP-linked genes (n=1,514).

(E) Occurrence of EBVSE-linked genes identified as c2/c4 DAP-linked DEGs associated with select EBNA binding sites relative to expected frequency due to random overlap (n=100 simulation trials, error bars depict mean +/- standard deviation). Random samples were size-matched relative to each EBNA-associated gene list.

(F) Example gene of interest analysis for TRAF1, an EBVSE-linked gene identified as a c2/c4 DAP-linked DEG with phenotype-variable accessibility at multiple EBNA binding sites.

See also Figures S39-S42, S44-S47

961  
962  
963  
964  
965  
966  
967  
968  
969  
970  
971  
972  
973  
974  
975  
976



977  
978  
979 **Figure 8. Discovery and characterization of EBV-driven transcriptomic dynamics in**  
980 **FCRL4<sup>+</sup> / TBX21<sup>+</sup> Tissue-Like Memory (TLM) B cells**

981 (A) Unbiased clustering of Day 5 scRNA assay processed using biological zero-preserving  
982 imputation by adaptive thresholding of low-rank approximation (ALRA; see ([Linderman et al.,](#)  
983 [2022](#))). Early infection model cluster numbering (top panel) and key markers of the EBV-induced  
984 pseudo-GC reaction are depicted (bottom-left column). A non-GC cluster of FCRL4<sup>+</sup> / TBX21<sup>+</sup>  
985 / CXCR3<sup>+</sup> B cells, consistent with TLM B cells, was also identified (bottom-right column).

986 (B) Hierarchically ordered phenotypes from imputed Day 5 data based on expression  
987 representative model state genes and top markers of the TLM B phenotype. With respect to the  
988 depicted genes, the TLM B state shares greater similarity to non-B cell lineages than other  
989 infected B cell states. Annotations are provided for TLM B cell markers genes, which include  
990 previously identified lineage markers (e.g., *ITGAX/CD11c*).

991 (C) Identification of the TLM B phenotype in ALRA-imputed Day 0 scRNA assay. Cells matching  
992 this phenotype from Day 0 and Day 5 were extracted and merged to evaluate differential gene  
993 expression pre- and post-EBV infection.

994 (D) Differential gene expression in TLM B cells in response to EBV infection.

995 (E) Expression of genes involved in nervous system development (GO:0007399, FDR = 0.0075)  
996 and tube morphogenesis (GO:0035239, FDR = 0.035) within TLM-like B cells before (d0) and  
997 after (d5, d8) EBV infection.

998 See also *Figure S43, S44*

999 **References**  
1000

1001 Alfieri, C., Birkenbach, M., and Kieff, E. (1991). Early events in Epstein-Barr virus infection of human B  
1002 lymphocytes. *Virology* 181, 595-608.

1003 Allday, M.J., Bazot, Q., and White, R.E. (2015). The EBNA3 family: two oncoproteins and a tumour  
1004 suppressor that are central to the biology of EBV in B cells. *Epstein Barr Virus Volume 2*, 61-117.

1005 Altmann, M., Pich, D., Ruiss, R., Wang, J., Sugden, B., and Hammerschmidt, W. (2006). Transcriptional  
1006 activation by EBV nuclear antigen 1 is essential for the expression of EBV's transforming genes.  
1007 *Proceedings of the National Academy of Sciences* 103, 14188-14193.

1008 Anderson, L.J., and Longnecker, R. (2008). EBV LMP2A provides a surrogate pre-B cell receptor signal  
1009 through constitutive activation of the ERK/MAPK pathway. *The Journal of general virology* 89, 1563.

1010 Arvey, A., Tempera, I., Tsai, K., Chen, H.-S., Tikhmyanova, N., Klichinsky, M., Leslie, C., and Lieberman,  
1011 P.M. (2012). An atlas of the Epstein-Barr virus transcriptome and epigenome reveals host-virus regulatory  
1012 interactions. *Cell host & microbe* 12, 233-245.

1013 Babcock, G.J.D., L.L.; Volk, M.; Thorley-Lawson, D.A. (1998). EBV Persistence in Memory B Cells In  
1014 Vivo. *Immunity* 9, 395-404.

1015 Banerjee, S., Lu, J., Cai, Q., Sun, Z., Jha, H.C., and Robertson, E.S. (2014). EBNA3C augments Pim-1  
1016 mediated phosphorylation and degradation of p21 to promote B-cell proliferation. *PLoS Pathog* 10,  
1017 e1004304.

1018 Bartkova, J., Rezaei, N., Liontos, M., Karakaidos, P., Kletsas, D., Issaeva, N., Vassiliou, L.-V.F., Kolettas,  
1019 E., Niforou, K., and Zoumpourlis, V.C. (2006). Oncogene-induced senescence is part of the  
1020 tumorigenesis barrier imposed by DNA damage checkpoints. *Nature* 444, 633-637.

1021 Bird, A.G.M., S.M.; Britton, S. (1981). Cyclosporin A promotes spontaneous outgrowth in vitro of Epstein-  
1022 Barr virus-induced B-cell lines. *Nature* 289, 300-301.

1023 Bjornevik, K., Cortese, M., Healy, B.C., Kuhle, J., Mina, M.J., Leng, Y., Elledge, S.J., Niebuhr, D.W.,  
1024 Scher, A.I., and Munger, K.L. (2022). Longitudinal analysis reveals high prevalence of Epstein-Barr virus  
1025 associated with multiple sclerosis. *Science*.

1026 Buenrostro, J.D., Wu, B., Litzenburger, U.M., Ruff, D., Gonzales, M.L., Snyder, M.P., Chang, H.Y., and  
1027 Greenleaf, W.J. (2015). Single-cell chromatin accessibility reveals principles of regulatory variation.  
1028 *Nature* 523, 486-490.

1029 Cahir-McFarland, E.D., Carter, K., Rosenwald, A., Giltnane, J.M., Henrickson, S.E., Staudt, L.M., and  
1030 Kieff, E. (2004). Role of NF- $\kappa$ B in cell survival and transcription of latent membrane protein 1-expressing  
1031 or Epstein-Barr virus latency III-infected cells. *Journal of virology* 78, 4108-4119.

1032 Calender, A., Billaud, M., Aubry, J.-P., Banchereau, J., Vuillaume, M., and Lenoir, G.M. (1987). Epstein-  
1033 Barr virus (EBV) induces expression of B-cell activation markers on in vitro infection of EBV-negative B-  
1034 lymphoma cells. *Proceedings of the National Academy of Sciences* 84, 8060-8064.

1035 Canaan, A., Haviv, I., Urban, A.E., Schulz, V.P., Hartman, S., Zhang, Z., Palejev, D., Deisseroth, A.B.,  
1036 Lacy, J., and Snyder, M. (2009). EBNA1 regulates cellular gene expression by binding cellular promoters.  
1037 *Proceedings of the National Academy of Sciences* 106, 22421-22426.

1038 Cao, J., Cusanovich, D.A., Ramani, V., Aghamirzaie, D., Pliner, H.A., Hill, A.J., Daza, R.M., McFaline-  
1039 Figueroa, J.L., Packer, J.S., and Christiansen, L. (2018). Joint profiling of chromatin accessibility and  
1040 gene expression in thousands of single cells. *Science* 361, 1380-1385.

1041 Cheah, M.S., Ley, T.J., Tronick, S.R., and Robbins, K.C. (1986). fgr proto-oncogene mRNA induced in B  
1042 lymphocytes by Epstein-Barr virus infection. *Nature* 319, 238-240.

1043 Chen, S., Lake, B.B., and Zhang, K. (2019). High-throughput sequencing of the transcriptome and  
1044 chromatin accessibility in the same cell. *Nature biotechnology* 37, 1452-1457.

1045 Clark, S.J., Argelaguet, R., Kapourani, C.-A., Stubbs, T.M., Lee, H.J., Alda-Catalinas, C., Krueger, F.,  
1046 Sanguinetti, G., Kelsey, G., and Marioni, J.C. (2018). scNMT-seq enables joint profiling of chromatin  
1047 accessibility DNA methylation and transcription in single cells. *Nature communications* 9, 1-9.

1048 Cohen, J.I., Fauci, A.S., Varmus, H., and Nabel, G.J. (2011). Epstein-Barr virus: an important vaccine  
1049 target for cancer prevention. *Science translational medicine* 3, 107fs107-107fs107.

1050 Cohen, J.I., Wang, F., Mannick, J., and Kieff, E. (1989). Epstein-Barr virus nuclear protein 2 is a key  
1051 determinant of lymphocyte transformation. *Proceedings of the National Academy of Sciences* 86, 9558-  
1052 9562.

1053 Courtois-Cox, S., Jones, S.L., and Cichowski, K. (2008). Many roads lead to oncogene-induced  
1054 senescence. *Oncogene* 27, 2801-2809.

1055 Davis, R.S. (2007). Fc receptor-like molecules. *Annu Rev Immunol* 25, 525-560.

1056 Deisenroth, C., and Zhang, Y. (2010). Ribosome biogenesis surveillance: probing the ribosomal protein-  
1057 Mdm2-p53 pathway. *Oncogene* 29, 4253-4260.

1058 Devergne, O., Hatzivassiliou, E., Izumi, K.M., Kaye, K.M., Kleijnen, M.F., Kieff, E., and Mosialos, G.  
1059 (1996). Association of TRAF1, TRAF2, and TRAF3 with an Epstein-Barr virus LMP1 domain important for  
1060 B-lymphocyte transformation: role in NF- $\kappa$ B activation. *Molecular and cellular biology* 16, 7098-7108.

1061 Devergne, O., McFarland, E.C., Mosialos, G., Izumi, K.M., Ware, C.F., and Kieff, E. (1998). Role of the  
1062 TRAF binding site and NF- $\kappa$ B activation in Epstein-Barr virus latent membrane protein 1-induced cell  
1063 gene expression. *Journal of virology* 72, 7900-7908.

1064 Dheekollu, J., Wiedmer, A., Ayyanathan, K., Deakyne, J.S., Messick, T.E., and Lieberman, P.M. (2021).  
1065 Cell-cycle-dependent EBNA1-DNA crosslinking promotes replication termination at oriP and viral episome  
1066 maintenance. *Cell* 184, 643-654. e613.

1067 Di Micco, R., Sulli, G., Dobreva, M., Lontos, M., Botrugno, O.A., Gargiulo, G., Dal Zuffo, R., Matti, V.,  
1068 d'Ario, G., and Montani, E. (2011). Interplay between oncogene-induced DNA damage response and  
1069 heterochromatin in senescence and cancer. *Nature cell biology* 13, 292-302.

1070 Dorfman, D.M., Hwang, E.S., Shahsafaei, A., and Glimcher, L.H. (2004). T-bet, a T-cell-associated  
1071 transcription factor, is expressed in a subset of B-cell lymphoproliferative disorders. *American journal of  
1072 clinical pathology* 122, 292-297.

1073 Durand, N.C., Robinson, J.T., Shamim, M.S., Machol, I., Mesirov, J.P., Lander, E.S., and Aiden, E.L.  
1074 (2016). Juicebox provides a visualization system for Hi-C contact maps with unlimited zoom. *Cell systems*  
1075 3, 99-101.

1076 Efremova, M., and Teichmann, S.A. (2020). Computational methods for single-cell omics across  
1077 modalities. *Nature methods* 17, 14-17.

1078 Eliopoulos, A.G., Waites, E.R., Blake, S.M., Davies, C., Murray, P., and Young, L.S. (2003). TRAF1 is a  
1079 critical regulator of JNK signaling by the TRAF-binding domain of the Epstein-Barr virus-encoded latent  
1080 infection membrane protein 1 but not CD40. *Journal of virology* 77, 1316-1328.

1081 Epstein, M., Achong, B., and Barr, Y. (1964). Virus particles in cultured lymphoblasts from Burkitt's  
1082 lymphoma. *Lancet*, 702-703.

1083 Fish, K., Comoglio, F., Shaffer, A.L., Ji, Y., Pan, K.-T., Scheich, S., Oellerich, A., Doebele, C., Ikeda, M.,  
1084 and Schaller, S.J. (2020). Rewiring of B cell receptor signaling by Epstein-Barr virus LMP2A.  
1085 *Proceedings of the National Academy of Sciences* 117, 26318-26327.

1086 Forte, E., and Luftig, M.A. (2009). MDM2-dependent inhibition of p53 is required for Epstein-Barr virus B-  
1087 cell growth transformation and infected-cell survival. *Journal of virology* 83, 2491-2499.

1088 Freudenthaler, M., Voll, R.E., Binder, S.C., Keller, B., and Warnatz, K. (2020). Naive-and memory-like  
1089 CD21low B cell subsets share core phenotypic and signaling characteristics in systemic autoimmune  
1090 disorders. *The Journal of Immunology* 205, 2016-2025.

1091 Fries, K.L., Miller, W.E., and Raab-Traub, N. (1999). The A20 protein interacts with the Epstein–Barr virus  
1092 latent membrane protein 1 (LMP1) and alters the LMP1/TRAF1/TRADD complex. *Virology* 264, 159-166.

1093 Gan, L., Seki, A., Shen, K., Iyer, H., Han, K., Hayer, A., Wollman, R., Ge, X., Lin, J.R., and Dey, G.  
1094 (2019). The lysosomal GPCR-like protein GPR137B regulates Rag and mTORC1 localization and activity.  
1095 *Nature cell biology* 21, 614-626.

1096 Gao, J., Xia, L., Lu, M., Zhang, B., Chen, Y., Xu, R., and Wang, L. (2012). TM7SF1 (GPR137B): a novel  
1097 lysosome integral membrane protein. *Molecular biology reports* 39, 8883-8889.

1098 Glaros, V., Rauschmeier, R., Artemov, A.V., Reinhardt, A., Ols, S., Emmanouilidi, A., Gustafsson, C.,  
1099 You, Y., Mirabello, C., and Björklund, Å.K. (2021). Limited access to antigen drives generation of early B  
1100 cell memory while restraining the plasmablast response. *Immunity* 54, 2005-2023. e2010.

1101 Glück, S., Guey, B., Gulen, M.F., Wolter, K., Kang, T.-W., Schmacke, N.A., Bridgeman, A., Rehwinkel, J.,  
1102 Zender, L., and Ablasser, A. (2017). Innate immune sensing of cytosolic chromatin fragments through  
1103 cGAS promotes senescence. *Nature cell biology* 19, 1061-1070.

1104 Greenfeld, H., Takasaki, K., Walsh, M.J., Ersing, I., Bernhardt, K., Ma, Y., Fu, B., Ashbaugh, C.W., Cabo,  
1105 J., and Mollo, S.B. (2015). TRAF1 coordinates polyubiquitin signaling to enhance Epstein-Barr virus  
1106 LMP1-mediated growth and survival pathway activation. *PLoS pathogens* 11, e1004890.

1107 Guasparri, I., Bubman, D., and Cesarman, E. (2008). EBV LMP2A affects LMP1-mediated NF- $\kappa$ B  
1108 signaling and survival of lymphoma cells by regulating TRAF2 expression. *Blood, The Journal of the*  
1109 *American Society of Hematology* 111, 3813-3820.

1110 Guo, R., Jiang, C., Zhang, Y., Govande, A., Trudeau, S.J., Chen, F., Fry, C.J., Puri, R., Wolinsky, E., and  
1111 Schineller, M. (2020). MYC controls the Epstein-Barr virus lytic switch. *Molecular cell* 78, 653-669. e658.

1112 Han, I., Harada, S., Weaver, D., Xue, Y., Lane, W., Orstavik, S., Skalhegg, B., and Kieff, E. (2001).  
1113 EBNA-LP associates with cellular proteins including DNA-PK and HA95. *Journal of virology* 75, 2475-  
1114 2481.

1115 Hao, Y., Hao, S., Andersen-Nissen, E., Mauck III, W.M., Zheng, S., Butler, A., Lee, M.J., Wilk, A.J.,  
1116 Darby, C., and Zager, M. (2021). Integrated analysis of multimodal single-cell data. *Cell*.

1117 Harada, S., and Kieff, E. (1997). Epstein-Barr virus nuclear protein LP stimulates EBNA-2 acidic domain-  
1118 mediated transcriptional activation. *Journal of virology* 71, 6611-6618.

1119 Henderson, S., Rowe, M., Gregory, C., Croom-Carter, D., Wang, F., Longnecker, R., Kieff, E., and  
1120 Rickinson, A. (1991). Induction of bcl-2 expression by Epstein-Barr virus latent membrane protein 1  
1121 protects infected B cells from programmed cell death. *Cell* 65, 1107-1115.

1122 Henle, W., Diehl, V., Kohn, G., Zur Hausen, H., and Henle, G. (1967). Herpes-type virus and  
1123 chromosome marker in normal leukocytes after growth with irradiated Burkitt cells. *Science* 157, 1064-  
1124 1065.

1125 Hodgkin, P.D., Lee, J.-H., and Lyons, A.B. (1996). B cell differentiation and isotype switching is related to  
1126 division cycle number. *Journal of Experimental Medicine* 184, 277-281.

1127 Hoffmann, A., Levchenko, A., Scott, M.L., and Baltimore, D. (2002). The I $\kappa$ B-NF- $\kappa$ B signaling module:  
1128 temporal control and selective gene activation. *science* 298, 1241-1245.

1129 Honjo, K., Won, W.-J., King, R.G., Ianov, L., Crossman, D.K., Easlick, J.L., Shakhmatov, M.A., Khass, M.,  
1130 Vale, A.M., Stephan, R.P., et al. (2020). Fc Receptor-Like 6 (FCRL6) Discloses Progenitor B Cell  
1131 Heterogeneity That Correlates With Pre-BCR Dependent and Independent Pathways of Natural Antibody  
1132 Selection. *Frontiers in Immunology* 11.

1133 Humme, S., Reisbach, G., Feederle, R., Delecluse, H.-J., Bousset, K., Hammerschmidt, W., and  
1134 Schepers, A. (2003). The EBV nuclear antigen 1 (EBNA1) enhances B cell immortalization several  
1135 thousandfold. *Proceedings of the National Academy of Sciences* 100, 10989-10994.

1136 Jenks, S.A., Cashman, K.S., Zumaquero, E., Marigorta, U.M., Patel, A.V., Wang, X., Tomar, D., Woodruff,  
1137 M.C., Simon, Z., and Bugrovsky, R. (2018). Distinct effector B cells induced by unregulated toll-like

1138 receptor 7 contribute to pathogenic responses in systemic lupus erythematosus. *Immunity* 49, 725-739.  
1139 e726.

1140 Jiang, S., and Mortazavi, A. (2018). Integrating ChIP-seq with other functional genomics data. *Briefings in*  
1141 *functional genomics* 17, 104-115.

1142 Jiang, S., Zhou, H., Liang, J., Gerdt, C., Wang, C., Ke, L., Schmidt, S.C., Narita, Y., Ma, Y., and Wang, S.  
1143 (2017). The Epstein-Barr virus regulome in lymphoblastoid cells. *Cell host & microbe* 22, 561-573. e564.

1144 Johannsen, E., Luftig, M., Chase, M.R., Weicksel, S., Cahir-McFarland, E., Illanes, D., Sarracino, D., and  
1145 Kieff, E. (2004). Proteins of purified Epstein-Barr virus. *Proceedings of the National Academy of Sciences*  
1146 101, 16286-16291.

1147 Johnson, J.L., Rosenthal, R.L., Knox, J.J., Myles, A., Naradikian, M.S., Madej, J., Kostiv, M., Rosenfeld,  
1148 A.M., Meng, W., and Christensen, S.R. (2020). The transcription factor T-bet resolves memory B cell  
1149 subsets with distinct tissue distributions and antibody specificities in mice and humans. *Immunity* 52, 842-  
1150 855. e846.

1151 Jones, D., Benjamin, R.J., Shahsafaei, A., and Dorfman, D.M. (2000). The chemokine receptor CXCR3 is  
1152 expressed in a subset of B-cell lymphomas and is a marker of B-cell chronic lymphocytic leukemia. *Blood*,  
1153 *The Journal of the American Society of Hematology* 95, 627-632.

1154 Junker, J.P., and van Oudenaarden, A. (2014). Every cell is special: genome-wide studies add a new  
1155 dimension to single-cell biology. *Cell* 157, 8-11.

1156 Kilger, E., Kieser, A., Baumann, M., and Hammerschmidt, W. (1998). Epstein-Barr virus-mediated B-cell  
1157 proliferation is dependent upon latent membrane protein 1, which simulates an activated CD40 receptor.  
1158 *The EMBO journal* 17, 1700-1709.

1159 Kim, U., Qin, X.-F., Gong, S., Stevens, S., Luo, Y., Nussenzweig, M., and Roeder, R.G. (1996). The B-  
1160 cell-specific transcription coactivator OCA-B/OBF-1/Bob-1 is essential for normal production of  
1161 immunoglobulin isotypes. *Nature* 383, 542-547.

1162 King, H.W., Orban, N., Riches, J.C., Clear, A.J., Warnes, G., Teichmann, S.A., and James, L.K. (2021).  
1163 Single-cell analysis of human B cell maturation predicts how antibody class switching shapes selection  
1164 dynamics. *Science Immunology* 6, eabe6291.

1165 Knutson, J.C. (1990). The level of c-fgr RNA is increased by EBNA-2, an Epstein-Barr virus gene required  
1166 for B-cell immortalization. *Journal of virology* 64, 2530-2536.

1167 Krynetskaia, N.F., Phadke, M.S., Jadhav, S.H., and Krynetskiy, E.Y. (2009). Chromatin-associated  
1168 proteins HMGB1/2 and PDIA3 trigger cellular response to chemotherapy-induced DNA damage.  
1169 *Molecular cancer therapeutics* 8, 864-872.

1170 Kwak, I.H., Kim, H.S., Choi, O.R., Ryu, M.S., and Lim, I.K. (2004). Nuclear accumulation of globular actin  
1171 as a cellular senescence marker. *Cancer research* 64, 572-580.

1172 Laichalk, L.L., and Thorley-Lawson, D.A. (2005). Terminal differentiation into plasma cells initiates the  
1173 replicative cycle of Epstein-Barr virus *in vivo*. *J Virol* 79, 1296-1307.

1174 Lamontagne, R.J., Soldan, S.S., Su, C., Wiedmer, A., Won, K.J., Lu, F., Goldman, A.R., Wickramasinghe,  
1175 J., Tang, H.-Y., Speicher, D.W., et al. (2021). A multi-omics approach to Epstein-Barr virus  
1176 immortalization of B-cells reveals EBNA1 chromatin pioneering activities targeting nucleotide metabolism.  
1177 *PLOS Pathogens* 17, e1009208.

1178 Lanz, T.V., Brewer, R.C., Ho, P.P., Moon, J.-S., Jude, K.M., Fernandez, D., Fernandes, R.A., Gomez,  
1179 A.M., Nadj, G.-S., Bartley, C.M., et al. (2022). Clonally Expanded B Cells in Multiple Sclerosis Bind EBV  
1180 EBNA1 and GlialCAM. *Nature*.

1181 Lenain, C., de Graaf, C.A., Pagie, L., Visser, N.L., de Haas, M., de Vries, S.S., Peric-Hupkes, D., van  
1182 Steensel, B., and Peeper, D.S. (2017). Massive reshaping of genome–nuclear lamina interactions during  
1183 oncogene-induced senescence. *Genome research* 27, 1634-1644.

1184 Lessard, F., Igelmann, S., Trahan, C., Huot, G., Saint-Germain, E., Mignacca, L., Del Toro, N., Lopes-  
1185 Paciencia, S., Le Calvé, B., and Montero, M. (2018). Senescence-associated ribosome biogenesis  
1186 defects contributes to cell cycle arrest through the Rb pathway. *Nature cell biology* 20, 789-799.

1187 Li, H., Borrego, F., Nagata, S., and Tolnay, M. (2016). Fc receptor-like 5 expression distinguishes two  
1188 distinct subsets of human circulating tissue-like memory B cells. *The Journal of Immunology* 196, 4064-  
1189 4074.

1190 Lindahl, T., Adams, A., Bjursell, G., Bornkamm, G.W., Kaschka-Dierich, C., and Jahn, U. (1976).  
1191 Covalently closed circular duplex DNA of Epstein-Barr virus in a human lymphoid cell line. *Journal of*  
1192 *molecular biology* 102, 511-530.

1193 Linderman, G.C., Zhao, J., Roulis, M., Bielecki, P., Flavell, R.A., Nadler, B., and Kluger, Y. (2022). Zero-  
1194 preserving imputation of single-cell RNA-seq data. *Nature Communications* 13, 1-11.

1195 Ling, P.D., Peng, R.S., Nakajima, A., Yu, J.H., Tan, J., Moses, S.M., Yang, W.H., Zhao, B., Kieff, E., and  
1196 Bloch, K.D. (2005). Mediation of Epstein-Barr virus EBNA-LP transcriptional coactivation by Sp100. *The*  
1197 *EMBO journal* 24, 3565-3575.

1198 Liu, T. (2014). Use model-based analysis of ChIP-Seq (MACS) to analyze short reads generated by  
1199 sequencing protein-DNA interactions in embryonic stem cells. In *Stem Cell Transcriptional Networks*  
1200 (Springer), pp. 81-95.

1201 Longnecker, R.M., Kieff, E., and Cohen, J.I. (2013). Epstein-barr virus. In *Fields Virology: Sixth Edition*  
1202 (Wolters Kluwer Health Adis (ESP)).

1203 Lu, F., Chen, H.-S., Kossenkov, A.V., DeWispeleare, K., Won, K.-J., and Lieberman, P.M. (2016). EBNA2  
1204 drives formation of new chromosome binding sites and target genes for B-cell master regulatory  
1205 transcription factors RBP-jk and EBF1. *PLoS pathogens* 12, e1005339.

1206 Lu, F., Wikramasinghe, P., Norseen, J., Tsai, K., Wang, P., Showe, L., Davuluri, R.V., and Lieberman,  
1207 P.M. (2010). Genome-wide analysis of host-chromosome binding sites for Epstein-Barr Virus Nuclear  
1208 Antigen 1 (EBNA1). *Virology journal* 7, 1-17.

1209 Luftig, M., Prinarakis, E., Yasui, T., Tsichritzis, T., Cahir-McFarland, E., Inoue, J.-I., Nakano, H., Mak,  
1210 T.W., Yeh, W.-C., and Li, X. (2003). Epstein-Barr virus latent membrane protein 1 activation of NF-κB  
1211 through IRAK1 and TRAF6. *Proceedings of the National Academy of Sciences* 100, 15595-15600.

1212 Lünenmann, A., Rowe, M., and Nadal, D. (2015). Innate immune recognition of EBV. *Epstein Barr Virus*  
1213 Volume 2, 265-287.

1214 Luo, Y., and Roeder, R.G. (1995). Cloning, functional characterization, and mechanism of action of the B-  
1215 cell-specific transcriptional coactivator OCA-B. *Molecular and cellular biology* 15, 4115-4124.

1216 Lupton, S., and Levine, A.J. (1985). Mapping genetic elements of Epstein-Barr virus that facilitate  
1217 extrachromosomal persistence of Epstein-Barr virus-derived plasmids in human cells. *Molecular and*  
1218 *Cellular Biology* 5, 2533-2542.

1219 Ma, S., Zhang, B., LaFave, L.M., Earl, A.S., Chiang, Z., Hu, Y., Ding, J., Brack, A., Kartha, V.K., and Tay,  
1220 T. (2020). Chromatin potential identified by shared single-cell profiling of RNA and chromatin. *Cell* 183,  
1221 1103-1116. e1120.

1222 Macosko, E.Z., Basu, A., Satija, R., Nemesh, J., Shekhar, K., Goldman, M., Tirosh, I., Bialas, A.R.,  
1223 Kamitaki, N., and Martersteck, E.M. (2015). Highly parallel genome-wide expression profiling of individual  
1224 cells using nanoliter droplets. *Cell* 161, 1202-1214.

1225 Mannick, J., Cohen, J., Birkenbach, M., Marchini, A., and Kieff, E. (1991). The Epstein-Barr virus nuclear  
1226 protein encoded by the leader of the EBNA RNAs is important in B-lymphocyte transformation. *Journal of*  
1227 *virology* 65, 6826-6837.

1228 Martin, H.J., Lee, J.M., Walls, D., and Hayward, S.D. (2007). Manipulation of the toll-like receptor 7  
1229 signaling pathway by Epstein-Barr virus. *Journal of virology* 81, 9748-9758.

1230 Martina, J.A., Chen, Y., Gucek, M., and Puertollano, R. (2012). MTORC1 functions as a transcriptional  
1231 regulator of autophagy by preventing nuclear transport of TFEB. *Autophagy* 8, 903-914.

1232 Maruo, S., Zhao, B., Johannsen, E., Kieff, E., Zou, J., and Takada, K. (2011). Epstein-Barr virus nuclear  
1233 antigens 3C and 3A maintain lymphoblastoid cell growth by repressing p16INK4A and p14ARF  
1234 expression. *Proceedings of the National Academy of Sciences* 108, 1919-1924.

1235 Matsuda, G., Nakajima, K., Kawaguchi, Y., Yamanashi, Y., and Hirai, K. (2003). Epstein-Barr virus (EBV)  
1236 nuclear antigen leader protein (EBNA-LP) forms complexes with a cellular anti-apoptosis protein Bcl-2 or  
1237 its EBV counterpart BHRF1 through HS1-associated protein X-1. *Microbiology and immunology* 47, 91-  
1238 99.

1239 McClellan, M.J., Wood, C.D., Ojeniyi, O., Cooper, T.J., Kanhere, A., Arvey, A., Webb, H.M., Palermo,  
1240 R.D., Harth-Hertle, M.L., Kempkes, B., *et al.* (2013). Modulation of enhancer looping and differential gene  
1241 targeting by Epstein-Barr virus transcription factors directs cellular reprogramming. *PLoS Pathog* 9,  
1242 e1003636.

1243 McFadden, K., Hafez, A.Y., Kishton, R., Messinger, J.E., Nikitin, P.A., Rathmell, J.C., and Luftig, M.A.  
1244 (2016). Metabolic stress is a barrier to Epstein-Barr virus-mediated B-cell immortalization. *Proceedings of*  
1245 *the National Academy of Sciences* 113, E782-E790.

1246 McInnes, L., Healy, J., and Melville, J. (2018). Umap: Uniform manifold approximation and projection for  
1247 dimension reduction. *arXiv preprint arXiv:180203426*.

1248 McLean, C.Y., Bristor, D., Hiller, M., Clarke, S.L., Schaar, B.T., Lowe, C.B., Wenger, A.M., and Bejerano,  
1249 G. (2010). GREAT improves functional interpretation of cis-regulatory regions. *Nature biotechnology* 28,  
1250 495-501.

1251 Messinger, J.E., Dai, J., Stanland, L.J., Price, A.M., and Luftig, M.A. (2019). Identification of Host  
1252 Biomarkers of Epstein-Barr Virus Latency IIb and Latency III. *mBio* 10.

1253 Minamitani, T., Yasui, T., Ma, Y., Zhou, H., Okuzaki, D., Tsai, C.-Y., Sakakibara, S., Gewurz, B.E., Kieff,  
1254 E., and Kikutani, H. (2015). Evasion of affinity-based selection in germinal centers by Epstein-Barr virus  
1255 LMP2A. *Proceedings of the National Academy of Sciences* 112, 11612-11617.

1256 Mitchell, S., Roy, K., Zangle, T.A., and Hoffmann, A. (2018). Nongenetic origins of cell-to-cell variability in  
1257 B lymphocyte proliferation. *Proc Natl Acad Sci U S A* 115, E2888-E2897.

1258 Miyashita, E.M., Yang, B., Babcock, G.J., and Thorley-Lawson, D.A. (1997). Identification of the site of  
1259 Epstein-Barr virus persistence in vivo as a resting B cell. *Journal of virology* 71, 4882-4891.

1260 Moir, S., Ho, J., Malaspina, A., Wang, W., DiPoto, A.C., O'Shea, M.A., Roby, G., Kottilil, S., Arthos, J.,  
1261 and Proschan, M.A. (2008). Evidence for HIV-associated B cell exhaustion in a dysfunctional memory B  
1262 cell compartment in HIV-infected viremic individuals. *The Journal of experimental medicine* 205, 1797-  
1263 1805.

1264 Mrozek-Gorska, P., Buschle, A., Pich, D., Schwarzmayr, T., Fechtner, R., Scialdone, A., and  
1265 Hammerschmidt, W. (2019). Epstein-Barr virus reprograms human B lymphocytes immediately in the  
1266 prelatent phase of infection. *Proc Natl Acad Sci U S A* 116, 16046-16055.

1267 Muehlinghaus, G., Cigliano, L., Huehn, S., Peddinghaus, A., Leyendeckers, H., Hauser, A.E., Hiepe, F.,  
1268 Radbruch, A., Arce, S., and Manz, R.A. (2005). Regulation of CXCR3 and CXCR4 expression during  
1269 terminal differentiation of memory B cells into plasma cells. *Blood* 105, 3965-3971.

1270 Nagelkerke, A., Sieuwerts, A.M., Bussink, J., Sweep, F., Look, M.P., Foekens, J.A., Martens, J., and  
1271 Span, P.N. (2014). LAMP3 is involved in tamoxifen resistance in breast cancer cells through the  
1272 modulation of autophagy. *Endocr Relat Cancer* 21, 101-112.

1273 Nicholas, M.W., Dooley, M.A., Hogan, S.L., Anolik, J., Looney, J., Sanz, I., and Clarke, S.H. (2008). A  
1274 novel subset of memory B cells is enriched in autoreactivity and correlates with adverse outcomes in SLE.  
1275 *Clinical immunology* 126, 189-201.

1276 Nikitin, P.A., Yan, C.M., Forte, E., Bocedi, A., Tourigny, J.P., White, R.E., Allday, M.J., Patel, A., Dave,  
1277 S.S., and Kim, W. (2010). An ATM/Chk2-mediated DNA damage-responsive signaling pathway  
1278 suppresses Epstein-Barr virus transformation of primary human B cells. *Cell host & microbe* 8, 510-522.

1279 Nilsson, K., Klein, G., Henle, W., and Henle, G. (1971). The establishment of lymphoblastoid lines from  
1280 adult and fetal human lymphoid tissue and its dependence on EBV. *International Journal of Cancer* 8,  
1281 443-450.

1282 Nishimura, K., Kumazawa, T., Kuroda, T., Katagiri, N., Tsuchiya, M., Goto, N., Furumai, R., Murayama,  
1283 A., Yanagisawa, J., and Kimura, K. (2015). Perturbation of ribosome biogenesis drives cells into  
1284 senescence through 5S RNP-mediated p53 activation. *Cell reports* 10, 1310-1323.

1285 Nonoyama, M., and Pagano, J.S. (1972). Separation of Epstein-Barr virus DNA from large chromosomal  
1286 DNA in non-virus-producing cells. *Nature New Biology* 238, 169-171.

1287 O'Dea, E.L., Barken, D., Peralta, R.Q., Tran, K.T., Werner, S.L., Kearns, J.D., Levchenko, A., and  
1288 Hoffmann, A. (2007). A homeostatic model of IkappaB metabolism to control constitutive NF-kappaB  
1289 activity. *Mol Syst Biol* 3, 111.

1290 Osorio, D., and Cai, J.J. (2021). Systematic determination of the mitochondrial proportion in human and  
1291 mice tissues for single-cell RNA-sequencing data quality control. *Bioinformatics* 37, 963-967.

1292 Osorio, D., Yu, X., Yu, P., Serpedin, E., and Cai, J.J. (2019). Single-cell RNA sequencing of a European  
1293 and an African lymphoblastoid cell line. *Sci Data* 6, 112.

1294 Osorio, D., Yu, X., Zhong, Y., Li, G., Serpedin, E., Huang, J.Z., and Cai, J.J. (2020). Single-cell  
1295 expression variability implies cell function. *Cells* 9, 14.

1296 Parker, G.A., Crook, T., Bain, M., Sara, E.A., Farrell, P.J., and Allday, M.J. (1996). Epstein-Barr virus  
1297 nuclear antigen (EBNA) 3C is an immortalizing oncoprotein with similar properties to adenovirus E1A and  
1298 papillomavirus E7. *Oncogene* 13, 2541-2549.

1299 Paschos, K., Parker, G.A., Watanatanasup, E., White, R.E., and Allday, M.J. (2012). BIM promoter  
1300 directly targeted by EBNA3C in polycomb-mediated repression by EBV. *Nucleic acids research* 40, 7233-  
1301 7246.

1302 Peng, R., Moses, S.C., Tan, J., Kremmer, E., and Ling, P.D. (2005). The Epstein-Barr virus EBNA-LP  
1303 protein preferentially coactivates EBNA2-mediated stimulation of latent membrane proteins expressed  
1304 from the viral divergent promoter. *Journal of virology* 79, 4492-4505.

1305 Pich, D., Mrozek-Gorska, P., Bouvet, M., Sugimoto, A., Akidil, E., Grundhoff, A., Hamperl, S., Ling, P.D.,  
1306 and Hammerschmidt, W. (2019). First days in the life of naive human B lymphocytes infected with  
1307 Epstein-Barr virus. *MBio* 10, e01723-01719.

1308 Pope, J., Horne, M., and Scott, W. (1968). Transformation of foetal human leukocytes in vitro by filtrates  
1309 of a human leukaemic cell line containing herpes-like virus. *International journal of cancer* 3, 857-866.

1310 Portis, T., and Longnecker, R. (2004). Epstein-Barr virus (EBV) LMP2A mediates B-lymphocyte survival  
1311 through constitutive activation of the Ras/PI3K/Akt pathway. *Oncogene* 23, 8619-8628.

1312 Price, A.M., Dai, J., Bazot, Q., Patel, L., Nikitin, P.A., Djavadian, R., Winter, P.S., Salinas, C.A., Barry,  
1313 A.P., Wood, K.C., et al. (2017). Epstein-Barr virus ensures B cell survival by uniquely modulating  
1314 apoptosis at early and late times after infection. *Elife* 6.

1315 Price, A.M., and Luftig, M.A. (2015). To be or not IIb: a multi-step process for Epstein-Barr virus latency  
1316 establishment and consequences for B cell tumorigenesis. *PLoS Pathog* 11, e1004656.

1317 Qadir, F.S., Saad; Dominguez-Bendala, Juan (2019). 3D Plotting of scRNAseq data using Seurat objects  
1318 (1.3) (Zenodo).

1319 Qadir, M.M.F., Álvarez-Cubela, S., Klein, D., van Dijk, J., Muñiz-Anquela, R., Moreno-Hernández, Y.B.,  
1320 Lanzoni, G., Sadiq, S., Navarro-Rubio, B., and García, M.T. (2020). Single-cell resolution analysis of the  
1321 human pancreatic ductal progenitor cell niche. *Proceedings of the National Academy of Sciences* 117,  
1322 10876-10887.

1323 Qiu, X., Mao, Q., Tang, Y., Wang, L., Chawla, R., Pliner, H.A., and Trapnell, C. (2017). Reversed graph  
1324 embedding resolves complex single-cell trajectories. *Nature methods* 14, 979.

1325 Quinlan, A.R., and Hall, I.M. (2010). BEDTools: a flexible suite of utilities for comparing genomic features.  
1326 *Bioinformatics* 26, 841-842.

1327 Raab-Traub, N. (2007). EBV-induced oncogenesis. *Human herpesviruses: biology, therapy, and*  
1328 *immunoprophylaxis*.

1329 Raj, A., Peskin, C.S., Tranchina, D., Vargas, D.Y., and Tyagi, S. (2006). Stochastic mRNA synthesis in  
1330 mammalian cells. *PLoS Biol* 4, e309.

1331 Raj, A., Rifkin, S.A., Andersen, E., and Van Oudenaarden, A. (2010). Variability in gene expression  
1332 underlies incomplete penetrance. *Nature* 463, 913-918.

1333 Raj, A., and Van Oudenaarden, A. (2008). Nature, nurture, or chance: stochastic gene expression and its  
1334 consequences. *Cell* 135, 216-226.

1335 Rakhmanov, M., Keller, B., Gutenberger, S., Foerster, C., Hoenig, M., Driessen, G., van der Burg, M., van  
1336 Dongen, J.J., Wiech, E., and Visentini, M. (2009). Circulating CD21low B cells in common variable  
1337 immunodeficiency resemble tissue homing, innate-like B cells. *Proceedings of the National Academy of*  
1338 *Sciences* 106, 13451-13456.

1339 Ramesh, A., Schubert, R.D., Greenfield, A.L., Dandekar, R., Loudermilk, R., Sabatino, J.J., Koelzer, M.T.,  
1340 Tran, E.B., Koshal, K., and Kim, K. (2020). A pathogenic and clonally expanded B cell transcriptome in  
1341 active multiple sclerosis. *Proceedings of the National Academy of Sciences* 117, 22932-22943.

1342 Ramírez, F., Bhardwaj, V., Arrigoni, L., Lam, K.C., Grüning, B.A., Villaveces, J., Habermann, B., Akhtar,  
1343 A., and Manke, T. (2018). High-resolution TADs reveal DNA sequences underlying genome organization  
1344 in flies. *Nature communications* 9, 1-15.

1345 Ressing, M.E., van Gent, M., Gram, A.M., Hooykaas, M.J., Piersma, S.J., and Wiertz, E.J. (2015).  
1346 Immune evasion by Epstein-Barr virus. *Epstein Barr Virus Volume* 2, 355-381.

1347 Rickinson, A., and Kieff, E. (2007). Epstein-Barr virus, p 2655–2700. *Fields virology* 2.

1348 Robertson, E.S., Grossman, S., Johannsen, E., Miller, C., Lin, J., Tomkinson, B., and Kieff, E. (1995).  
1349 Epstein-Barr virus nuclear protein 3C modulates transcription through interaction with the sequence-  
1350 specific DNA-binding protein J kappa. *Journal of virology* 69, 3108-3116.

1351 Robinson, J.T., Thorvaldsdóttir, H., Winckler, W., Guttman, M., Lander, E.S., Getz, G., and Mesirov, J.P.  
1352 (2011). Integrative genomics viewer. *Nature biotechnology* 29, 24-26.

1353 Roy, K., Mitchell, S., Liu, Y., Ohta, S., Lin, Y.-s., Metzig, M.O., Nutt, S.L., and Hoffmann, A. (2019). A  
1354 regulatory circuit controlling the dynamics of NF $\kappa$ B cRel transitions B cells from proliferation to plasma cell  
1355 differentiation. *Immunity* 50, 616-628. e616.

1356 Rubtsova, K., Rubtsov, A.V., van Dyk, L.F., Kappler, J.W., and Marrack, P. (2013). T-box transcription  
1357 factor T-bet, a key player in a unique type of B-cell activation essential for effective viral clearance.  
1358 *Proceedings of the National Academy of Sciences* 110, E3216-E3224.

1359 Saha, A., Jha, H.C., Upadhyay, S.K., and Robertson, E.S. (2015). Epigenetic silencing of tumor  
1360 suppressor genes during in vitro Epstein–Barr virus infection. *Proceedings of the National Academy of*  
1361 *Sciences* 112, E5199-E5207.

1362 Sandberg, M., Hammerschmidt, W., and Sugden, B. (1997). Characterization of LMP-1's association with  
1363 TRAF1, TRAF2, and TRAF3. *Journal of Virology* 71, 4649-4656.

1364 Satija, R., Farrell, J.A., Gennert, D., Schier, A.F., and Regev, A. (2015). Spatial reconstruction of single-  
1365 cell gene expression data. *Nature biotechnology* 33, 495-502.

1366 Satpathy, A.T., Granja, J.M., Yost, K.E., Qi, Y., Meschi, F., McDermott, G.P., Olsen, B.N., Mumbach,  
1367 M.R., Pierce, S.E., and Corces, M.R. (2019). Massively parallel single-cell chromatin landscapes of  
1368 human immune cell development and intratumoral T cell exhaustion. *Nature biotechnology* 37, 925-936.

1369 Scharer, C.D., Blalock, E.L., Mi, T., Barwick, B.G., Jenks, S.A., Deguchi, T., Cashman, K.S., Neary, B.E.,  
1370 Patterson, D.G., and Hicks, S.L. (2019). Epigenetic programming underpins B cell dysfunction in human  
1371 SLE. *Nature immunology* 20, 1071-1082.

1372 Schubart, D.B., Rolink, A., Kosco-Vilbois, M.H., Botteri, F., and Matthias, P. (1996). B-cell-specific  
1373 coactivator OBF-1/OCA-B/Bob1 required for immune response and germinal centre formation. *Nature*  
1374 383, 538-542.

1375 Settembre, C., Di Malta, C., Polito, V.A., Arencibia, M.G., Vetrini, F., Erdin, S., Erdin, S.U., Huynh, T.,  
1376 Medina, D., and Colella, P. (2011). TFEB links autophagy to lysosomal biogenesis. *science* 332, 1429-  
1377 1433.

1378 Shair, K.H., Schnegg, C.I., and Raab-Traub, N. (2008). EBV latent membrane protein 1 effects on  
1379 plakoglobin, cell growth, and migration. *Cancer research* 68, 6997-7005.

1380 Shalek, A.K., Satija, R., Adiconis, X., Gertner, R.S., Gaublomme, J.T., Raychowdhury, R., Schwartz, S.,  
1381 Yosef, N., Malboeuf, C., and Lu, D. (2013). Single-cell transcriptomics reveals bimodality in expression  
1382 and splicing in immune cells. *Nature* 498, 236-240.

1383 Shannon, P., Markiel, A., Ozier, O., Baliga, N.S., Wang, J.T., Ramage, D., Amin, N., Schwikowski, B., and  
1384 Ideker, T. (2003). Cytoscape: a software environment for integrated models of biomolecular interaction  
1385 networks. *Genome research* 13, 2498-2504.

1386 Shapiro, E., Biezuner, T., and Linnarsson, S. (2013). Single-cell sequencing-based technologies will  
1387 revolutionize whole-organism science. *Nature Reviews Genetics* 14, 618-630.

1388 Simpson, E.H. (1951). The interpretation of interaction in contingency tables. *Journal of the Royal  
1389 Statistical Society: Series B (Methodological)* 13, 238-241.

1390 Sinclair, A.J., Palmero, I., Peters, G., and Farrell, P. (1994). EBNA-2 and EBNA-LP cooperate to cause  
1391 G0 to G1 transition during immortalization of resting human B lymphocytes by Epstein-Barr virus. *The  
1392 EMBO journal* 13, 3321-3328.

1393 Skalska, L., White, R.E., Franz, M., Ruhmann, M., and Allday, M.J. (2010). Epigenetic repression of  
1394 p16INK4A by latent Epstein-Barr virus requires the interaction of EBNA3A and EBNA3C with CtBP. *PLoS  
1395 pathogens* 6, e1000951.

1396 Smith, N., Tierney, R., Wei, W., Vockerodt, M., Murray, P.G., Woodman, C.B., and Rowe, M. (2013).  
1397 Induction of interferon-stimulated genes on the IL-4 response axis by Epstein-Barr virus infected human b  
1398 cells; relevance to cellular transformation. *PLoS One* 8, e64868.

1399 Sohn, H.W., Krueger, P.D., Davis, R.S., and Pierce, S.K. (2011). FcRL4 acts as an adaptive to innate  
1400 molecular switch dampening BCR signaling and enhancing TLR signaling. *Blood, The Journal of the  
1401 American Society of Hematology* 118, 6332-6341.

1402 SoRelle, E.D., Dai, J., Bonglack, E.N., Heckenberg, E.M., Zhou, J.Y., Giamberardino, S.N., Bailey, J.A.,  
1403 Gregory, S.G., Chan, C., and Luftig, M.A. (2021). Single-cell RNA-seq reveals transcriptomic  
1404 heterogeneity mediated by host-pathogen dynamics in lymphoblastoid cell lines. *Elife* 10, e62586.

1405 Stros, M., Ozaki, T., Baciková, A., Kageyama, H., and Nakagawara, A. (2002). HMGB1 and HMGB2 cell-  
1406 specifically down-regulate the p53-and p73-dependent sequence-specific transactivation from the human  
1407 Bax gene promoter. *Journal of Biological Chemistry* 277, 7157-7164.

1408 Stuart, T., Butler, A., Hoffman, P., Hafemeister, C., Papalexi, E., Mauck III, W.M., Hao, Y., Stoeckius, M.,  
1409 Smibert, P., and Satija, R. (2019). Comprehensive integration of single-cell data. *Cell* 177, 1888-1902.  
1410 e1821.

1411 Stuart, T., Srivastava, A., Lareau, C., and Satija, R. (2020). Multimodal single-cell chromatin analysis with  
1412 Signac. *BioRxiv*.

1413 Stuart, T., Srivastava, A., Madad, S., Lareau, C.A., and Satija, R. (2021). Single-cell chromatin state  
1414 analysis with Signac. *Nature Methods*, 1-9.

1415 Styles, C.T., Bazot, Q., Parker, G.A., White, R.E., Paschos, K., and Allday, M.J. (2017). EBV  
1416 epigenetically suppresses the B cell-to-plasma cell differentiation pathway while establishing long-term  
1417 latency. *PLoS Biol* 15, e2001992.

1418 Suan, D., Kräutler, N.J., Maag, J.L., Butt, D., Bourne, K., Hermes, J.R., Avery, D.T., Young, C., Statham,  
1419 A., and Elliott, M. (2017). CCR6 defines memory B cell precursors in mouse and human germinal centers,  
1420 revealing light-zone location and predominant low antigen affinity. *Immunity* 47, 1142-1153. e1144.

1421 Sun, C.C., and Thorley-Lawson, D.A. (2007). Plasma cell-specific transcription factor XBP-1s binds to  
1422 and transactivates the Epstein-Barr virus BZLF1 promoter. *J Virol* 81, 13566-13577.

1423 Szabo, S.J., Kim, S.T., Costa, G.L., Zhang, X., Fathman, C.G., and Glimcher, L.H. (2000). A novel  
1424 transcription factor, T-bet, directs Th1 lineage commitment. *Cell* 100, 655-669.

1425 Szymula, A., Palermo, R.D., Bayoumy, A., Groves, I.J., Ba Abdullah, M., Holder, B., and White, R.E.  
1426 (2018). Epstein-Barr virus nuclear antigen EBNA-LP is essential for transforming naive B cells, and  
1427 facilitates recruitment of transcription factors to the viral genome. *PLoS pathogens* 14, e1006890.

1428 Taylor, G.M., Raghuvanshi, S.K., Rowe, D.T., Wadowsky, R.M., and Rosendorff, A. (2011). Endoplasmic  
1429 reticulum stress causes EBV lytic replication. *Blood, The Journal of the American Society of Hematology*  
1430 118, 5528-5539.

1431 Taylor, J.J., Pape, K.A., Steach, H.R., and Jenkins, M.K. (2015). Apoptosis and antigen affinity limit  
1432 effector cell differentiation of a single naïve B cell. *Science* 347, 784-787.

1433 Thorley-Lawson, D.A. (2001). Epstein-Barr virus: exploiting the immune system. *Nature Reviews  
1434 Immunology* 1, 75-82.

1435 Thorley-Lawson, D.A., and Gross, A. (2004). Persistence of the Epstein-Barr virus and the origins of  
1436 associated lymphomas. *New England Journal of Medicine* 350, 1328-1337.

1437 Thorley-Lawson, D.A., and Mann, K.P. (1985). Early events in Epstein-Barr virus infection provide a  
1438 model for B cell activation. *The Journal of experimental medicine* 162, 45-59.

1439 Tomkinson, B., Robertson, E., and Kieff, E. (1993). Epstein-Barr virus nuclear proteins EBNA-3A and  
1440 EBNA-3C are essential for B-lymphocyte growth transformation. *Journal of virology* 67, 2014-2025.

1441 Tosato, G., Blaese, R., and Yarchoan, R. (1985). Relationship between immunoglobulin production and  
1442 immortalization by Epstein Barr virus. *The Journal of Immunology* 135, 959-964.

1443 Trapnell, C. (2015). Defining cell types and states with single-cell genomics. *Genome research* 25, 1491-  
1444 1498.

1445 Tsai, K., Thikmyanova, N., Wojcechowskyj, J.A., Delecluse, H.-J., and Lieberman, P.M. (2011). EBV  
1446 tegument protein BNRF1 disrupts DAXX-ATRX to activate viral early gene transcription. *PLoS pathogens*  
1447 7, e1002376.

1448 Uchida, J., Yasui, T., Takaoka-Shichijo, Y., Muraoka, M., Kulwichit, W., Raab-Traub, N., and Kikutani, H.  
1449 (1999). Mimicry of CD40 signals by Epstein-Barr virus LMP1 in B lymphocyte responses. *Science* 286,  
1450 300-303.

1451 Verstappen, G.M., Ice, J.A., Bootsma, H., Pringle, S., Haacke, E.A., de Lange, K., van der Vries, G.B.,  
1452 Hickey, P., Vissink, A., and Spijkervet, F.K. (2020). Gene expression profiling of epithelium-associated  
1453 FcRL4+ B cells in primary Sjögren's syndrome reveals a pathogenic signature. *Journal of autoimmunity*  
1454 109, 102439.

1455 Wang, A., Welch, R., Zhao, B., Ta, T., Keleş, S., and Johannsen, E. (2015). Epstein-Barr virus nuclear  
1456 antigen 3 (EBNA3) proteins regulate EBNA2 binding to distinct RBPJ genomic sites. *Journal of virology*  
1457 90, 2906-2919.

1458 Wang, C., Li, D., Zhang, L., Jiang, S., Liang, J., Narita, Y., Hou, I., Zhong, Q., Zheng, Z., and Xiao, H.  
1459 (2019). RNA sequencing analyses of gene expression during Epstein-Barr virus infection of primary B  
1460 lymphocytes. *Journal of virology* 93, e00226-00219.

1461 Wang, L.W., Jiang, S., and Gewurz, B.E. (2017). Epstein-Barr virus LMP1-mediated oncogenicity. *Journal*  
1462 of virology 91, e01718-01716.

1463 Wang, N.S., McHeyzer-Williams, L.J., Okitsu, S.L., Burris, T.P., Reiner, S.L., and McHeyzer-Williams,  
1464 M.G. (2012). Divergent transcriptional programming of class-specific B cell memory by T-bet and ROR $\alpha$ .  
1465 *Nature immunology* 13, 604-611.

1466 Wang, S., Wang, J., Kumar, V., Karnell, J.L., Naiman, B., Gross, P.S., Rahman, S., Zerrouki, K., Hanna,  
1467 R., and Morehouse, C. (2018). IL-21 drives expansion and plasma cell differentiation of autoreactive  
1468 CD11chiT-bet $+$  B cells in SLE. *Nature communications* 9, 1-14.

1469 Weiss, G.E., Crompton, P.D., Li, S., Walsh, L.A., Moir, S., Traore, B., Kayentao, K., Ongoiba, A.,  
1470 Doumbo, O.K., and Pierce, S.K. (2009). Atypical memory B cells are greatly expanded in individuals living  
1471 in a malaria-endemic area. *The Journal of Immunology* 183, 2176-2182.

1472 Wendel-Hansen, V., Rosén, A., and Klein, G. (1987). EBV-transformed lymphoblastoid cell lines down-  
1473 regulate ebna in parallel with secretory differentiation. *International journal of cancer* 39, 404-408.

1474 White, R.E., Groves, I.J., Turro, E., Yee, J., Kremmer, E., and Allday, M.J. (2010). Extensive co-operation  
1475 between the Epstein-Barr virus EBNA3 proteins in the manipulation of host gene expression and  
1476 epigenetic chromatin modification. *PloS one* 5, e13979.

1477 Wills, Q.F., Livak, K.J., Tipping, A.J., Enver, T., Goldson, A.J., Sexton, D.W., and Holmes, C. (2013).  
1478 Single-cell gene expression analysis reveals genetic associations masked in whole-tissue experiments.  
1479 *Nature biotechnology* 31, 748-752.

1480 Wilson, T.J., Presti, R.M., Tassi, I., Overton, E.T., Cella, M., and Colonna, M. (2007). FcRL6, a new ITIM-  
1481 bearing receptor on cytolytic cells, is broadly expressed by lymphocytes following HIV-1 infection. *Blood*  
1482 109, 3786-3793.

1483 Wolff, J., Bhardwaj, V., Nothjunge, S., Richard, G., Renschler, G., Gilsbach, R., Manke, T., Backofen, R.,  
1484 Ramírez, F., and Grüning, B.A. (2018). Galaxy HiCExplorer: a web server for reproducible Hi-C data  
1485 analysis, quality control and visualization. *Nucleic acids research* 46, W11-W16.

1486 Wolff, J., Rabbani, L., Gilsbach, R., Richard, G., Manke, T., Backofen, R., and Grüning, B.A. (2020).  
1487 Galaxy HiCExplorer 3: a web server for reproducible Hi-C, capture Hi-C and single-cell Hi-C data  
1488 analysis, quality control and visualization. *Nucleic acids research* 48, W177-W184.

1489 Wood, V., O'Neil, J., Wei, W., Stewart, S., Dawson, C., and Young, L. (2007). Epstein-Barr virus-encoded  
1490 EBNA1 regulates cellular gene transcription and modulates the STAT1 and TGF  $\beta$  signaling pathways.  
1491 *Oncogene* 26, 4135-4147.

1492 Wu, J., Xia, L., Yao, X., Yu, X., Tumas, K.C., Sun, W., Cheng, Y., He, X., Peng, Y.-c., and Singh, B.K.  
1493 (2020). The E3 ubiquitin ligase MARCH1 regulates antimalaria immunity through interferon signaling and  
1494 T cell activation. *Proceedings of the National Academy of Sciences* 117, 16567-16578.

1495 Wu, X., Xiao, Y., Zhou, Y., Zhou, Z., and Yan, W. (2019). LncRNA FOXP4-AS1 is activated by PAX5 and  
1496 promotes the growth of prostate cancer by sequestering miR-3184-5p to upregulate FOXP4. *Cell death &*  
1497 *disease* 10, 1-14.

1498 Wu, Y., Bressette, D., Carrell, J.A., Kaufman, T., Feng, P., Taylor, K., Gan, Y., Cho, Y.H., Garcia, A.D.,  
1499 and Gollatz, E. (2000). Tumor necrosis factor (TNF) receptor superfamily member TAC1 is a high affinity  
1500 receptor for TNF family members APRIL and BLyS. *Journal of Biological Chemistry* 275, 35478-35485.

1501 Yanai, H., Ban, T., Wang, Z., Choi, M.K., Kawamura, T., Negishi, H., Nakasato, M., Lu, Y., Hangai, S.,  
1502 and Koshiba, R. (2009). HMGB proteins function as universal sentinels for nucleic-acid-mediated innate  
1503 immune responses. *Nature* 462, 99-103.

1504 Yates, J.L., Warren, N., and Sugden, B. (1985). Stable replication of plasmids derived from Epstein-Barr  
1505 virus in various mammalian cells. *Nature* 313, 812-815.

1506 Yeo, L., Lom, H., Juarez, M., Snow, M., Buckley, C., Filer, A., Raza, K., and Scheel-Toellner, D. (2015).  
1507 Expression of FcRL4 defines a pro-inflammatory, RANKL-producing B cell subset in rheumatoid arthritis.  
1508 Annals of the rheumatic diseases 74, 928-935.

1509 Yetming, K.D., Lupey-Green, L.N., Biryukov, S., Hughes, D.J., Marendy, E.M., Miranda, J.L., and Sample,  
1510 J.T. (2020). The BHLF1 locus of Epstein-Barr virus contributes to viral latency and B-cell immortalization.  
1511 Journal of virology 94, e01215-01220.

1512 Young, L.S., Arrand, J.R., and Murray, P.G. (2007). EBV gene expression and regulation. Human  
1513 herpesviruses: biology, therapy, and immunoprophylaxis.

1514 Young, L.S., and Rickinson, A.B. (2004). Epstein-Barr virus: 40 years on. Nat Rev Cancer 4, 757-768.

1515 Zhao, B., Zou, J., Wang, H., Johannsen, E., Peng, C.-w., Quackenbush, J., Mar, J.C., Morton, C.C.,  
1516 Freedman, M.L., and Blacklow, S.C. (2011). Epstein-Barr virus exploits intrinsic B-lymphocyte  
1517 transcription programs to achieve immortal cell growth. Proceedings of the National Academy of Sciences  
1518 108, 14902-14907.

1519 Zheng, G.X., Terry, J.M., Belgrader, P., Ryvkin, P., Bent, Z.W., Wilson, R., Ziraldo, S.B., Wheeler, T.D.,  
1520 McDermott, G.P., and Zhu, J. (2017). Massively parallel digital transcriptional profiling of single cells.  
1521 Nature communications 8, 1-12.

1522 Zhou, H., Schmidt, S.C., Jiang, S., Willox, B., Bernhardt, K., Liang, J., Johannsen, E.C., Kharchenko, P.,  
1523 Gewurz, B.E., and Kieff, E. (2015). Epstein-Barr virus oncogene super-enhancers control B cell growth.  
1524 Cell host & microbe 17, 205-216.

1525 Zhu, C., Yu, M., Huang, H., Juric, I., Abnousi, A., Hu, R., Lucero, J., Behrens, M.M., Hu, M., and Ren, B.  
1526 (2019). An ultra high-throughput method for single-cell joint analysis of open chromatin and  
1527 transcriptome. Nature structural & molecular biology 26, 1063-1070.

1528